Published in final edited form as:

Nature. 2020 July ; 583(7816): 473–478. doi:10.1038/s41586-020-2370-1.

Structure of a nascent membrane protein as it folds on the Bam complex

David Tomasek[1,2], **Shaun Rawson**[3], **James Lee**[1,2,5], **Joseph S. Wzorek**[2,6], **Stephen C. Harrison**[3,4,*], **Zongli Li**[3,4,*], **Daniel Kahne**[1,2,3,*]

[1]Department of Molecular and Cellular Biology, Harvard University, Cambridge, MA 02138, USA

[2]Department of Chemistry and Chemical Biology, Harvard University, Cambridge, MA 02138, USA

[3]Department of Biological Chemistry and Molecular Pharmacology, Harvard Medical School, Boston, MA 02115, USA

[4]Howard Hughes Medical Institute, Boston, MA 02115, USA

[5]Present address: Laboratory of Membrane Biophysics and Biology, The Rockefeller University, New York, NY 10065, USA

[6]Present address: Novartis Institutes for BioMedical Research, Cambridge, MA 02139, USA

Abstract

Mitochondria, chloroplasts, and Gram-negative bacteria are encased in a double layer of membranes. The outer membrane contains proteins with a β-barrel structure[1,2]. β-barrels are sheets of β-strands wrapped into a cylinder with the first strand hydrogen-bonded to the last strand. Conserved multi-subunit molecular machines fold and insert these proteins into the outer membrane[3–5]. One subunit of the machines is itself a β-barrel protein that plays a central role in folding other β-barrels. In Gram-negative bacteria, the β-barrel assembly machine (Bam) consists of the β-barrel protein BamA and four lipoproteins[5–8]. To understand how the Bam complex accelerates folding without using exogenous energy (e.g., ATP)[9], we trapped folding intermediates on the machine. We report here the structure of the Bam complex folding BamA itself. The BamA catalyst ($BamA^{M}$, for $BamA^{machine}$) forms an asymmetric hybrid β-barrel with the BamA substrate ($BamA^{S}$). The N-terminal edge of $BamA^{M}$ has an antiparallel hydrogen-bonded interface with the C-terminal edge of $BamA^{S}$, consistent with previous crosslinking studies[10–12]; the other edges of $BamA^{M}$ and $BamA^{S}$ are close to each other but curl inward and do not pair. Six hydrogen

*Correspondence to be addressed to: harrison@crystal.harvard.edu (S.C.H.); zongli_li@hms.harvard.edu (Z.L.); kahne@chemistry.harvard.edu (D.K.).

Author contributions: D.T. designed and all performed biochemical experiments with assistance from J.L. and J.S.W. at early stages of the project. D.T. performed protein purification and screened samples using negative-stain electron microscopy. Z.L. collected cryo-EM data. Z.L. and S.R. processed cryo-EM data. D.T. and S.R. built the atomic models. D.K. and S.C.H. supervised the project. D.T. and D.K. wrote the manuscript and all authors contributed to editing.

Competing interests: The authors declare no competing interests.

Data availability: The electron microscopy maps will be deposited into the Electron Microscopy Data Bank under accession codes EMD-20969 (4.1 Å) and EMD-21313 (6.5 Å). The atomic model, built from the 4.1 Å map, will be deposited into the Protein Data Bank under accession code PDB 6V05. All data are available in the manuscript or the supplementary materials.

bonds in a membrane environment make the interface between the two proteins very stable. This stability allows folding but creates a high kinetic barrier to substrate release once folding has finished. Features at each end of the substrate overcome the barrier and promote release by stepwise exchange of hydrogen bonds. This mechanism of substrate-assisted product release explains how the Bam complex can stably associate with the substrate during folding and then turn over rapidly when folding is complete.

Keywords

Bam complex; outer membrane protein; β-barrel; protein folding; cryo-electron microscopy

Structures of the Bam complex from bacteria have provided clues to the mechanism of substrate folding[13–17]. A striking finding in some of these structures is that the BamA β-barrel component of the machine (Fig. 1a) is present in an open state with unpaired N- and C-terminal β-strands[13–15,17]. This open seam was proposed to pair with substrate β-strands by hydrogen bonding to facilitate β-sheet formation, leading to a general model in which folded portions of the substrate undergo "budding" through the open seam into the membrane[13,18–20]. Crosslinking experiments have provided support for interaction of β-barrel substrates with the edges of the open seam[10–12], but no model for folding has addressed how the Bam complex catalyzes rapid and repeated assembly of substrates into β-barrels in the absence of an exogenous source of energy[9,21,22]. Paired β-strands in a membrane are so stable that the kinetic barrier to disrupt them is enormous. To explain how the folding process is catalyzed requires structures of folding intermediates trapped on the Bam complex.

Capturing substrates on the Bam complex

We developed an approach to trap partially folded substrates on the Bam complex of *Escherichia coli*. To do so, we selected BamA as a substrate of the Bam complex, so that BamA within the machine ($BamA^M$) folds other copies of BamA. We generated a series of substrates ($BamA^S$), each of which lacked one of the eight extracellular loops (Fig. 1b and Extended Data Fig. 1a). We reasoned that loop deletions could prevent proper formation of β-hairpins, resulting in slowed folding. To test this possibility, we assessed susceptibility of the substrate variants to the periplasmic protease DegP to determine whether folding stalled in the periplasm before membrane insertion[23]. Removal of loops within the C-terminal half of $BamA^S$ resulted in DegP susceptibility, but removal of loops within the N-terminal half did not (Fig. 1c-d). Likewise, urea extraction experiments, which indicate whether a substrate is properly integrated in the membrane, showed that substrates lacking loops in the C-terminal half of the protein could be extracted by the denaturant, while substrates lacking N-terminal loops could not (Fig. 1e). Both experiments are consistent with the idea that the C-terminal half of the $BamA^S$ β-barrel, but not the N-terminal half, is needed for integration into the membrane and hence is assembled early in the folding process.

To assess whether the substrates accumulate on the Bam complex during folding, we incorporated the photocrosslinkable amino acid para-benzoyl phenylalanine (pBPA) near the N-terminal β-strand of the seam in $BamA^M$ (at residue S439). We have previously found

that, upon irradiation with ultraviolet light, pBPA introduced at this position forms crosslinks to the C-terminal region of a different substrate, LptD, during its folding[12]. Importantly, substrates that fold slowly form stronger crosslinks to $BamA^M$ than wild-type substrates because they have a longer residence time. Here, we tested crosslinking from $BamA^M$ (S439pBPA) to loop-deleted substrates; in these substrates, we also removed POTRA domains 3, 4, and 5 because, as we have shown, removal of these domains prevents $BamA^S$ from forming BamABCDE complexes if it does complete folding[24]. We found that loop-deleted substrates indeed crosslinked strongly to the $BamA^M$ N-terminus (Fig. 1f). Taken together, these results show that removal of extracellular loops in $BamA^S$ leads to accumulation of the substrates on the machine, but either outside or within the membrane, depending on the stage in the folding process at which they stall. Our results are consistent with earlier reports showing that deletions of the extracellular loops of BamA lead to impaired cell growth and lower protein levels[25,26].

Structure of a substrate-engaged Bam complex

We chose the substrate with loop 1 removed ($BamA^S$-ΔL1) for structural studies because it accumulates at a late stage of folding, when it has already integrated into the membrane but remains associated with the Bam complex. To stabilize the interactions between $BamA^M$ and the folding substrate, we engineered a disulfide bond between the two proteins (Extended Data Fig. 1b-f and Extended Data Fig. 2a). The substrate used for structure determination appears capable of adopting a folded state under reducing conditions, although folding occurs slowly (Extended Data Fig. 2b). We purified the BamABCDE-$BamA^S$ complex (Extended Data Fig. 2c-d) and determined its structure by cryo-EM to an overall resolution of 4.1 Å (Extended Data Fig. 3, Fig. 1g, and Supplementary Table 1). The cryo-EM map contains density for all five components of the Bam complex and for the substrate (Fig. 2a-b and Extended Data Fig. 4). All β-strands of the $BamA^M$ β-barrel were resolved, as were all β-strands of the $BamA^S$ β-barrel except β1 and β2. Extracellular loop 1, which we removed from the substrate, would normally connect these two β-strands. The POTRA domains of the substrate were also not visible in the structure.

Using previously published X-ray crystallographic structures[15,27], we built atomic models into our cryo-EM map (Fig. 2c). The overall architecture of the Bam complex in its substrate-bound state is similar to that seen in substrate-free states[14–17], with the organization of the periplasmic components most closely resembling that of substrate-free structures containing a laterally-open form of BamA (Extended Data Fig. 5). Structures of the individual components are likewise similar to those already published (Extended Data Fig. 6). There are, however, notable conformational differences between the N-terminal segment of the $BamA^M$ β-barrel in our substrate-engaged complex and the corresponding segment in any of the substrate-free, lateral-open structures (Fig. 2d). Specifically, the first and second β-strands of $BamA^M$ in the substrate-engaged β-barrel bend outward, separating them more from the C-terminal β-strand than they are in the substrate-free β-barrel. Smaller deviations in β-strands 3, 4, and 5 allow the larger changes in β1 and β2, but all remaining β-strands superimposed well on previous structures of BamA (Fig. 2d and Extended Data Fig. 6).

Like the BamA^{M} β-barrel, the membrane-embedded BamA^{S}-ΔL1 β-barrel has a lateral opening. The location of BamA^{S} in the membrane is consistent with our biochemical experiments (Fig. 1). Density was absent for β1 and β2 of the substrate, presumably because deletion of loop 1, which would normally connect these two β-strands, prevented proper formation of the corresponding β-hairpin (Extended Data Fig. 7). Additionally, the POTRA domains of the substrate could not be resolved. However, the rest of the β-barrel closely resembled the folded form of BamA, suggesting that the substrate in the structure is an on-pathway intermediate (Extended Data Fig. 7). The N-terminal β-strand of BamA^{M} and the C-terminal β-strand of BamA^{S} are paired in an interaction that involves six hydrogen bonds (Fig. 2e-f), creating a BamA^{M}-BamA^{S} hybrid barrel with a continuous lumen.

Asymmetric interface between BamA^{M} and BamA^{S}

Whereas the C-terminal β-strand of BamA^{S} is captured by the N-terminal β-strand of BamA^{M}, the β-strands at the other ends of BamA^{S} and BamA^{M} are not hydrogen bonded (Fig. 3a-c). Instead, these ends curve inwards, so that the barrels make contact along their exterior surfaces that would normally contact membrane lipids. Given that we used a disulfide bond to tether the C-terminal region BamA^{M} to the N-terminal region of BamA^{S} to stabilize the complex during purification, it was possible that the asymmetric interface we observe in our structure reflected a non-native conformation of the complex. To address this, we determined another structure with the same substrate but using a cysteine tether introduced between the other ends of BamA^{M} and BamA^{S} (Extended Data Fig. 8). This 6.5 Å structure is remarkably similar to our 4.1 Å structure (Extended Data Fig. 8i), indicating that using cysteine tethers does not alter the overall conformation of the complex.

The asymmetry of the hybrid β-barrel implies that side chains within BamA^{S} that are oriented outward should be exposed to lipopolysaccharide (LPS) molecules in the membrane except near its N-terminus, which should be inaccessible to LPS. We tested this implication by incorporating pBPA at four sites oriented toward the exterior of BamA^{S} (Fig. 3c and Extended Data Fig. 9a-b), including at a site on the surface that curves inward (T467) in the hybrid β-barrel. After *in vivo* photocrosslinking, we purified the Bam-BamA^{S} complex and analyzed crosslinks from BamA^{S} to both LPS and BamA^{M} (Fig. 3d). The results showed that the T467pBPA substitution in BamA^{S}-ΔL1 yielded a crosslink to BamA^{M}, whereas the other substitutions (Y531pBPA, M741pBPA, F804pBPA) yielded crosslinks to LPS. These results agree with the finding from our structure that most of the substrate's exterior surface faces the membrane, whereas the N-terminal β-strands interact with BamA^{M}.

β-strands 1 and 2 of the substrate are not visible in our structure. To determine their location, we substituted F428 and F440 in BamA^{S}-ΔL1 with pBPA. We observed crosslinks from the substrate to BamA^{M} (Extended Data Fig. 9c-d). Based on where β-strand 3 is located in the structure, and because the periplasmic loop from β-strand 3 to β-strand 2 is not long enough to reach the accessory Bam subunits, we infer that β-strands 1 and 2 likely interact with the BamA^{M} β-barrel or POTRA domain 5 of BamA^{M}.

Although there is an unpaired edge at one end each of BamA^{M} and of BamA^{S}, inward curvature ensures that these edges face into the lumen of the hybrid barrel, where they are

solvated by water. The seal created by the hydrophobic interaction interface between $BamA^M$ and $BamA^S$ prevents entry of lipid molecules into the lumen (Fig. 3b-c). Early intermediates may not be able to curve around to form this interface, and indeed, we did not detect crosslinks to LPS using pBPA substitutions within $BamA^S$-ΔL5 or $BamA^S$-ΔL8 (Fig. 3d). This finding, combined with our results above, supports the notion that the polypeptide chain takes different routes during early and late folding rather than "budding" continuously from the $BamA^M$ β-barrel and into the membrane[11,20,23,28,29]. Sequential membrane insertion of hairpins would imply that the nonpolar side of any hairpin would always face lipid (Fig. 3c-d). Specifying the mechanism of early folding will require visualizing an early intermediate.

The interaction between the N-terminal β-strand of the $BamA^M$ β-barrel with the C-terminal edge of the $BamA^S$ β-barrel has direct implications for the folding mechanism. By binding the exposed N-terminal edge of $BamA^M$ as an extended β-strand, the C-terminus of the substrate forms a new edge to template binding of the subsequent β-strand in a process known as β-strand augmentation[30–32]. Therefore, folding will be directional, proceeding from the C-terminus to the N-terminus of the substrate. Based on crosslinking experiments, a sequential, C- to N-terminal folding model was proposed for the mitochondrial homolog Sam50[10]. We probed directional folding by generating six $BamA^S$ variants in which two extracellular loops had been removed (Fig. 3e). In each construct, removal of the loop closer to the C-terminus determined the overall susceptibility to protease digestion, which reports on membrane integration (Fig. 3f-g). These differences in proteolytic susceptibility allow us to conclude that the region including loop 8 folds before that including loop 5, and so forth. This finding establishes C- to N-terminal directional folding and is consistent with sequential β-strand augmentation.

Mechanism of substrate release

The six hydrogen bonds at the interface between the N-terminal β-strand of the $BamA^M$ β-barrel and the C-terminal β-strand of the $BamA^S$ β-barrel (Fig. 2e-f) prevent premature product release, but the strength of that interaction raises the question of how release occurs at all. In a membrane, disrupting a hydrogen bond costs approximately 4 kcal/mol[33,34]. Thus, the kinetic barrier to disrupting all six hydrogen bonds at once would be insurmountably high, even though the process is thermodynamically favorable.

Two unexpected features of the structure suggest a mechanism for substrate β-barrel closure and release. First, the edges of the two barrels at the folding end of the substrate do not engage in hydrogen bonding but instead turn inward toward the water-filled lumen of the hybrid barrel. Thus, no polar bonds to the machine need to be broken at that edge. Second, the register of the hydrogen bonds between the N-terminal β-strand of the $BamA^M$ β-barrel and the C-terminal β-strand of the $BamA^S$ β-barrel is not the same as it is between the N- and C-terminal β-strands of a folded BamA β-barrel[13,35]. The hydrogen-bonded residues on the $BamA^M$ side are largely the same as those at the seam of a closed β-barrel, but they interact with different residues in the C-terminal β-strand of the trapped substrate. In our structure, $BamA^M$ splays open at the extracellular end of its N-terminal β-strand (Fig. 2d), facilitating pairing with residues in the C-terminal β-strand of $BamA^S$ that precede those

paired with the N-terminal β-strand in the fully folded structure (compare Figs. 2f and 4a). This pairing creates an overhang at the end of the $BamA^S$ C-terminal β-strand (Fig. 4b-c) by steric clash with the loop between β-strands 14 and 15 of $BamA^S$. These observations suggest a stepwise model for how release occurs (Fig. 4d). When the N-terminal β-strand of $BamA^S$ adds to the substrate β-barrel, it approaches the C-terminal overhang (Fig. 4d). The N- and C-termini of the substrate begin to form hydrogen bonds, sequentially disrupting bonds between the substrate and the machine. Unlike concerted disruption, sequential displacement is energetically feasible. As hydrogen bonds form to close the substrate β-barrel, the C-terminal β-strand of the substrate peels away stepwise from its interaction with the N-terminal β-strand of the $BamA^M$ β-barrel. The accompanying relaxation of strain in the splayed N-terminal hairpin might accelerate the strand exchange.

We tested the implication of the strand-exchange mechanism as follows. First, we ruled out a special role for an invariant glycine present in BamA (G807 in *E. coli*) and homologs in mitochondria and chloroplasts, just at the boundary of the C-terminal overhang in our structure (Fig. 4e). Changing G807 to valine has been reported to cause outer membrane defects[36]. We made the G807V mutation to determine whether it prevents release of an otherwise wild-type $BamA^S$ but found no defects in its assembly (Fig. 4f-h), as judged by DegP sensitivity and by crosslinking. These results indicate that the G807V substitution alters BamA function rather than assembly.

Second, we made substrate variants with proline substitutions at positions 807, 808 or 809 in the overhanging C-terminal segment. Proline distorts the conformation and hydrogen bonding in a β-sheet. DegP did not degrade these proline-substituted substrates (Fig. 4f-g), implying that they undergo membrane integration. *In vivo* photocrosslinking to $BamA^M$ (Fig. 4h) showed that these substrates accumulate on the machine in a membrane-integrated state. Moreover, deleting the C-terminal residues (809–810) also caused late-stage assembly defects (Fig. 4f-h). These results suggest that forming hydrogen bonds between the C-terminal overhang and N-terminal β-strand of $BamA^S$ facilitates release of $BamA^S$ from $BamA^M$.

Discussion

The structure reported here supports the central idea of models in which substrates pass through the side of the BamA β-barrel into the membrane (Extended Data Fig. 10)[13,18–20]. It is also consistent with crosslinking studies showing that the C-terminal β-strand of the folding substrate interacts strongly with the N-terminal edge of the seam of the $BamA^M$ β-barrel[10–12]. Moreover, its two unexpected features—the unpaired edges at one junction and the hydrogen-bond register and overhang at the other—resolve problems posed by models postulating hydrogen-bonded arrays at both edges of the machine. Sequential replacement of each substrate-machine hydrogen bond by a substrate-substrate hydrogen bond yields a succession of rapid steps rather than a single, slow one. We believe that the β-barrel closure and release mechanism described here is general: other Bam substrates could have C-terminal overhangs (Supplementary Table 2) that, when bound to the machine, would protrude inside the hybrid barrel to engage their own N-termini. With this information, it

may be possible to design antibiotics that bind to features of BamA and inhibit β-barrel folding and release[37–40].

Methods

SDS-PAGE and immunoblotting.

Homemade Tris-HCl 4–20% polyacrylamide gradient gels or Mini-PROTEAN TGX 7.5% precast gels (BioRad) were used with Tris-glycine running buffer. 2× SDS sample buffer refers to a mixture containing 125 mM Tris (pH 6.8), 4% (wt/vol) SDS, 30% (vol/vol) glycerol, 0.005% bromophenol blue, and 5% (vol/vol) β-mercaptoethanol. SDS-PAGE analyses were performed at 200 V for 45 to 60 min. To analyze purified protein complexes for cryo-EM, SDS-PAGE was performed and followed by staining with Coomassie Brilliant Blue (Alfa Aesar). Coomassie-stained SDS-PAGE gels were imaged using the “Gel” feature of an Azure Biosystems C400 imager. For Western blotting, proteins were transferred onto Immun-Blot PVDF membranes (Bio-Rad) and then incubated with appropriate antibodies. All HRP conjugates were visualized with the Amersham ECL Prime Western blotting detection reagent (GE Healthcare). Western blots were imaged using the “lowest” sensitivity setting of the “Chemi” feature of an Azure Biosystems C400 imager. Uncropped immunoblots are available in Supplementary Figure 1.

Plasmids, strains, and oligonucleotides.

Plasmids, strains, and oligonucleotides used in this study are reported in Supplementary Tables 3, 4, and 5, respectively.

Analysis of cellular BamA levels.

Derivatives of a plasmid containing 6×His-BamA cloned into the pZS21 vector (pSK476) were generated to contain single loop deletions (pDT175-pDT182), double loop deletions (pDT260-pDT265), or C-terminal overhang mutations (pDT521, pDT536-pDT538, pDT550). MC4100 cells[41] and MC4100 *degP::cam* cells[23] were transformed with these plasmids. The resulting strains were grown in LB supplemented with 50 μg/mL kanamycin (for MC4100) or 50 μg/mL kanamycin and 30 μg/mL chloramphenicol (for MC4100 *degP::cam*) (37°C, 220 rpm). Once an OD600 of ~1.0 was reached, the cells from a 1 mL sample were collected by centrifugation (5,000 x g, 10 min, 4°C). The resulting cell pellets were resuspended in 80 μL of a 1:1 mixture of 2× SDS sample buffer and buffer containing 20 mM Tris-HCl pH 8.0 and 150 mM NaCl. After boiling for 10 min, the samples were applied to SDS-PAGE and analyzed via Western blotting. 6×His-BamA was detected by using a penta-His (HRP) antibody (Qiagen). RpoA was detected using a mouse anti-RpoA (*E. coli* RNA Polymerase α) primary antibody (BioLegend, clone 4RA2) followed by a sheep anti-mouse (HRP) secondary antibody (GE Healthcare).

Membrane extraction with urea.

Membrane extraction was performed in a manner as previously described[42]. MC4100 *degP::cam* strains were generated harboring the pZS21 vector encoding 6×His-BamA or derivatives containing single or double loop deletions. These strains were grown overnight in LB supplemented with 50 μg/mL kanamycin and 30 μg/mL chloramphenicol (37°C, 220

rpm). These cultures were used to inoculate 100 mL of LB with the same additives via 1:100 dilutions. The resulting cultures were grown (37°C, 220 rpm) until an OD600 of ~1.0 was reached. The cells were harvested via centrifugation (5,000 x g, 10 min, 4°C) and resuspended in 4 mL of resuspension solution (50 mM Tris-HCl pH 8.0, 10 μg/mL DNase). Cells were lysed via sonication (on and off at 10 second intervals for a total of 3 min on and 3 min off). The resulting lysate was centrifuged to pellet cell debris (5,000 x g, 10 min, 4°C). The supernatant was used to prepare normalized cell lysate suspensions to an A280 value of ~24 (assayed by using NanoDrop). An aliquot of each normalized lysate sample was removed, mixed 1:1 with 2× SDS sample buffer (containing β-mercaptoethanol), and boiled for 10 min. For each sample, 800 μL of the remaining lysate was transferred to 70.1 Ti ultracentrifuge tubes (Beckman Coulter) along with an additional 5 mL of 50 mM Tris-HCl pH 8.0. Membrane fractions were then isolated via ultracentrifugation (100,000 x g, 25 min, 4°C) using an Optima XE-90 ultracentrifuge (Beckman Coulter). The supernatant was discarded, and the membrane pellet was resuspended in 800 μL of 6 M urea. The resuspensions were incubated at 37°C for 1 hour. An aliquot of each sample, representative of total membrane protein content, was removed, mixed 1:1 with 2× SDS sample buffer (containing β-mercaptoethanol), and boiled for 10 min. The post-wash membrane pellet was isolated from the remainder of each sample via ultracentrifugation (100,000 x g, 45 min, 20°C) after addition of 5 mL of 50 mM Tris-HCl pH 8.0. The pellets were resuspended in 500 μL of water. An aliquot of each sample was removed, mixed 1:1 with 2× SDS sample buffer (containing β-mercaptoethanol), and boiled for 10 min. The samples were applied to SDS-PAGE and analyzed via Western blotting. 6×His-BamA was detected by using a penta-His (HRP) antibody (Qiagen). LptF was detected using LptF antiserum followed by a donkey anti-rabbit (HRP) secondary antibody (GE Healthcare). The source of rabbit anti-LptF antiserum has been previously reported[43].

In vivo photocrosslinking of BamA to substrates.

Photocrosslinking experiments are based on techniques as previously described[44,45], with modifications. The plasmid pSup-BpaRS-6TRN encodes an orthogonal tRNA and aminoacyl-tRNA synthetase to incorporate the unnatural amino acid pBPA at amber (TAG) stop codons[46]. This plasmid contains a chloramphenicol resistance cassette, so is not compatible with the MC4100 *degP::cam* strain. To circumvent this, we generated a variant of the pSup-BpaRS-6TRN plasmid that instead contains a spectinomycin resistance cassette. In brief, pSup-BpaRS-6TRN minus the chloramphenicol resistance cassette was amplified, and the spectinomycin resistance cassette was amplified from the pCDFDuet vector (EMD Millipore). The pSup-BpaRS-6TRN backbone and the spectinomycin resistance cassette were joined via Gibson assembly[47] to generate pSup-BpaRS-6TRN(spec^R) (pDT504).

6×His-BamA^M containing pBPA substitutions were cloned into the pZS21 vector to generate pJL77. 3×FLAG-tagged substrates were cloned into the pTrc99a vector to generate pDT209 (WT BamA^S); pDT201-pDT208 (single loop deletions); pDT268, pDT270, and pDT272 (double loop deletions); and pDT526, pDT558-pDT560, and pDT562 (C-terminal overhang mutants). The 3×FLAG-tagged substrates also contain deletion of POTRA domains 3, 4, and 5 (Δ172–421) to avoid the possibility of these substrates forming Bam complexes if they complete folding. The deletion does not prevent folding of an otherwise wild-type BamA[24],

and allows us to assess $BamA^S$ mutants in terms of their ability to fold rather than function within a Bam complex. In these constructs, POTRA domains 1 and 2 are retained since deletion of all five POTRA domains prevents an otherwise wild-type BamA from folding properly.

MC4100 *degP::cam* strains were generated, each harboring pSup-BpaRS-6TRN($spec^R$), pJL77, and one of the substrate-encoding plasmids. These strains were grown overnight in LB supplemented with 50 μg/mL carbenicillin, 50 μg/mL kanamycin, 50 μg/mL spectinomycin, and 0.2% (w/v) glucose (37°C, 220 rpm). These overnight cultures were diluted 1:100 into 100 mL of fresh LB containing the same additives minus glucose but supplemented with 0.8 mM H-p-Bz-Phe-OH (pBPA, Bachem), and were grown (37°C, 220 rpm) to OD600 ~0.35. After normalization by optical density, each culture was split in half, with one half used directly for irradiation with UV light at 365 nm for 10 min (on ice). Photocrosslinking was performed by using a UVP Blak-Ray B-100AP high-intensity UV lamp with a 100 W spot bulb. All cells were then pelleted by centrifugation (5,000 x g, 10 min, 4°C).

For protein purification, pellets were resuspended in 5 mL TBS (20 mM Tris-HCl pH 8.0, 300 mM NaCl) supplemented with 1% (w/v) Anzergent 3–14 (Anatrace), 20 mM imidazole (pH 8.0), 100 μg/mL lysozyme (Sigma-Aldrich), 1 mM PMSF (Sigma-Aldrich), and 50 μg/mL DNase I (Sigma-Aldrich). Cells were lysed via sonication (on and off at 10 second intervals for a total of 1 min and 30 sec on and 1 min and 30 sec off). The resulting lysate was centrifuged (10,000 x g, 10 min, 4°C). An aliquot of the supernatant was taken for analysis of 3×FLAG-$BamA^S$ expression levels via SDS-PAGE and immunoblotting using a monoclonal anti-FLAG M2-peroxidase (HRP) mouse antibody (Sigma-Aldrich). The remainder of the supernatant was incubated with Ni-nitrilotriacetic acid (NTA) resin on a rocking platform (1 hour, 4°C). After removal of unbound proteins, the resin was washed twice with 50 CV (column volumes) TBS containing 0.02% Anzergent 3–14 and 20 mM imidazole (pH 8.0). Samples were eluted with 5 CV TBS containing 0.02% Anzergent 3–14 and 200 mM imidazole (pH 8.0). Eluates were supplemented with 10% TCA by volume and incubated on ice for 20 min. Precipitated proteins were pelleted via centrifugation (21,130 x g, 10 min, 4°C). All samples were resuspended in a 1:1 mixture of 2× SDS loading dye (containing β-mercaptoethanol) and 1 M Tris pH 8.0. After boiling for 20 min, each sample was analyzed by SDS-PAGE and Western blotting. 6×His-$BamA^M$ was detected by using a penta-His (HRP) antibody (Qiagen). 3×FLAG-$BamA^S$ that was pulled down with 6×His-$BamA^M$ was detected by using a monoclonal anti-FLAG M2-peroxidase (HRP) antibody (Sigma-Aldrich).

In vivo photocrosslinking of BamA to LPS.

6×His-BamA containing pBPA substitutions were cloned into the pZS21 vector to generate pDT411, pDT416, and pDT421-pDT430. MC4100 strains were generated, each harboring pSup-BpaRS-6TRN (containing a chloramphenicol resistance cassette) and one of the plasmids encoding pBPA-substituted BamA. These strains were grown overnight in LB supplemented with 50 μg/mL kanamycin and 30 μg/mL chloramphenicol. These overnight cultures were diluted 1:100 into 100 mL of fresh LB containing the same additives

supplemented with 0.8 mM H-p-Bz-Phe-OH (pBPA, Bachem), and were grown (37°C, 220 rpm) to OD600 ~0.35. The protocols for UV irradiation and protein purification are the same as described above for *in vivo* photocrosslinking of $BamA^M$ to substrates.

In vivo photocrosslinking of substrates to LPS or $BamA^M$, followed by DSP crosslinking to the Bam complex.

In order to observe crosslinking from substrates to lipopolysaccharide or to $BamA^M$, a separate crosslinking protocol was devised to ensure that only substrates stalled on the Bam complex were assessed. In brief, we crosslinked the exterior surface of substrates to their surroundings (using incorporated pBPA) and then crosslinked stalled substrates to the Bam complex (using an amine-to-amine crosslinker). This was followed by purification of Bam-substrate complexes and release of the substrate with reducing agent (which breaks the amine-to-amine crosslinks), allowing assessment of UV-dependent crosslinks by SDS-PAGE and Western blotting.

The pJH114 plasmid[48] was modified to encode 3×FLAG-$BamA^M$ and BamD-8×His (while eliminating the 8×His tag on BamE), generating pDT340. 2×Strep-tagged $BamA^S$ substrates containing deletion of POTRA domains 3–5, deletion of an extracellular loop (L1, L3, L5, or L8), and a pBPA substitution (at T467, Y531, M741, or F804) were cloned into the pCDF vector to generate pDT436-pDT439 (T467pBPA), pDT451-pDT454 (Y531pBPA), pDT471-pDT474 (M741pBPA), and pDT476-pDT479 (F804pBPA). BL21(DE3) strains were generated harboring pSup-BpaRS-6TRN, pDT340, and one of the substrate-encoding plasmids.

These strains were grown overnight in LB supplemented with 50 μg/mL carbenicillin, 50 μg/mL spectinomycin, 30 μg/mL chloramphenicol, and 0.2% (w/v) glucose (28°C, 220 rpm). These overnight cultures were diluted 1:100 into 100 mL of fresh LB containing the same additives, and were grown (37°C, 220 rpm) to OD600 ~0.35. At this point, isopropyl β-D-1-thiogalactopyranoside (IPTG, VWR) and 0.8 mM H-p-Bz-Phe-OH (pBPA, Bachem) were added to final concentrations of 0.1 mM and 0.8 mM, respectively. The strains were grown for an additional 90 minutes. After normalization by optical density, each culture was split in half, with one half used directly for irradiation with UV light at 365 nm for 10 min (on ice). All cells were then pelleted by centrifugation (5,000 x g, 10 min, 4°C). Pellets were resuspended in 20 mL PBS (20 mM NaH_2PO_4 pH 7.2, 150 mM NaCl) and the amine-to-amine crosslinker dithiobis(succinimidyl propionate) (DSP, Thermo Fisher Scientific) was added to a final concentration of 0.5 mM. After incubation on a rocking platform (30 to 60 min, room temperature), the crosslinking reaction was quenched via addition of Tris-HCl to a final concentration of 20 mM. Cells were centrifuged (5,000 x g, 10 min, 4°C) and the pellets were frozen at −80°C prior to subsequent purification.

Protein purification was performed similarly as described for testing site-specific *in vivo* crosslinking without DSP crosslinking, with a few differences. The Ni-NTA wash step was performed using 50 CV TBS containing 0.1% Triton X-100 (Sigma-Aldrich), 0.1% SDS (J. T. Baker), and 40 mM imidazole (pH 8.0). The Ni-NTA elution step was performed using 5 CV TBS containing 200 mM imidazole (pH 8.0) and no detergent. Instead of using TCA precipitation, each sample was concentrated using an Amicon Ultra 0.5 mL 10 kDa

molecular-weight cutoff centrifugal concentrator (EMD Millipore). All samples were supplemented with an equal volume of 2× SDS loading dye (containing β-mercaptoethanol). After boiling for 10 min, each sample was analyzed by SDS-PAGE and Western blotting. 8×His-BamD was detected by using a penta-His (HRP) antibody (Qiagen). 2×Strep-BamA^S substrates were detected using a monoclonal Strep-Tag II (HRP) antibody (EMD Millipore). 3×FLAG-BamA^M was detected by using a monoclonal anti-FLAG M2-peroxidase (HRP) antibody (Sigma-Aldrich). Lipopolysaccharide was detected using a mouse monoclonal anti-lipopolysaccharide core primary antibody (Hycult Biotech, clone WN1 222–5) followed by a sheep anti-mouse (HRP) conjugate secondary antibody (GE Healthcare).

Assessing cysteine-to-cysteine crosslinking.

6×His-BamA^M containing a cysteine substitution was cloned into the pZS21 vector to generate pDT511-pDT513 (C-proximal cysteine mutant) and pDT400 (N-proximal cysteine mutant). 3×FLAG-tagged substrates (BamA^S containing deletion of POTRA domains 3–5, deletion of loop 1, and a cysteine substitution) were cloned into the pTrc99a vector to generate pDT514-pDT516 (N-proximal cysteine mutant) and pDT481 and pDT486-pDT490 (C-proximal cysteine mutant). Substrates containing the above but with POTRA domains 3–5 intact were cloned to generate pDT566-pDT568. MC4100 cells were transformed with one BamA^M-encoding plasmid and one substrate-encoding plasmid. The resulting strains were grown overnight in LB supplemented with 50 μg/mL carbenicillin, 50 μg/mL kanamycin, and 0.2% (w/v) glucose (37°C, 220 rpm). These overnight cultures were diluted 1:100 into 100 mL of fresh LB containing the same additives minus glucose, and were grown (37°C, 220 rpm) to OD600 ~0.5. Cells were then collected by centrifugation (4,200 x g, 10 min, 4°C). Cell pellets were resuspended in PBS (20 mM NaH_2PO_4 pH 7.2, 150 mM NaCl). TCEP-HCl (VWR) was then added at a final concentration of 2 mM, and cells were incubated on a rocking platform (20 min, room temperature). Cells were then centrifuged (5,000 x g, 10 min, 4°C) and again resuspended in PBS. To test for cysteine crosslinking, 1,2-bis(maleimido)ethane (BMOE, Thermo Fisher) was added at a final concentration of 0.5 mM. After incubation on a rocking platform (40 min, room temperature), the crosslinking reaction was quenched via addition of L-cysteine hydrochloride monohydrate (Alfa Aesar) to a final concentration of 10 mM. Cells were centrifuged (5,000 x g, 10 min, 4°C) and the pellets were frozen at −80°C prior to subsequent purification. To test disulfide bond formation in the absence of crosslinker, cells were frozen after the initial centrifugation step. In each sample, 6×His-BamA^M was purified and crosslinked adducts were detected by Western blotting as described for site-specific *in vivo* photocrosslinking experiments. β-mercaptoethanol was not added to samples used to assess disulfide formation in the absence of crosslinker.

Assessing heat modifiability of substrates.

2×Strep-BamA^S containing deletion of POTRA domains 3–5 and the C690S, C700S, and T467C mutations was cloned into the pTrc99a vector to generate pDT534. Another plasmid containing the same mutations, but with deletion of loop 1 (Δ430–439) was cloned to generate pDT535. The equivalent constructs with the E800C mutation were cloned to generate pDT509 (loop 1 intact) and pDT510 (loop 1 deleted). MC4100 cells were transformed with pDT534, pDT535, pDT509, or pDT510. The resulting strains were grown

overnight in LB supplemented with 50 μg/mL carbenicillin and 0.2% (w/v) glucose (37°C, 220 rpm). These overnight cultures were diluted 1:100 into 5 mL of fresh LB containing the same additives minus glucose, and were grown (37°C, 220 rpm) to OD600 ~0.4. Cells were then collected by centrifugation (4,200 x g, 10 min, 4°C) and resuspended in 2× SDS loading dye (containing β-mercaptoethanol). Each sample was divided into two, with one half boiled for 5 min and the other half remaining unboiled. All samples were analyzed by SDS-PAGE and Western blotting. 2×Strep-BamA^{S} was detected using a monoclonal Strep-Tag II (HRP) antibody (EMD Millipore).

Expression and crosslinking of substrate-bound Bam complex for cryo-EM.

The plasmid pJH114 was modified such that BamA^{M} contained the C690S and C700S substitutions, in addition F804C, generating pDT517. 2×Strep-BamA^{S} containing deletion of POTRA domains 3–5, deletion of loop 1, the C690S and C700S substitutions, and T467C, was cloned into the pBAD33 vector to generate pDT518. BL21(DE3) cells harboring pDT517 and pDT518 were grown overnight (37°C, 220 rpm) in LB supplemented with 50 μg/mL carbenicillin, 30 μg/mL chloramphenicol, and 0.2% glucose. This overnight culture was diluted 1:100 into 3 × 1.5 L of LB supplemented with 50 μg/mL carbenicillin and 30 μg/mL chloramphenicol. The resulting cultures were grown (37°C, 220 rpm) until an OD600 of ~0.7 was reached. At this point, the temperature was turned down to 30°C, and cells were allowed to continue shaking. After 20 min, protein expression was induced with isopropyl β-D-1-thiogalactopyranoside (IPTG, VWR) and L-(+)-arabinose (Alfa Aesar) at final concentrations of 0.2 mM and 0.1% (w/v), respectively. After three hours of additional shaking, cells were harvested via centrifugation (4,200 x g, 10 min, 4°C). Cell pellets were resuspended in PBS (20 mM NaH_2PO_4 pH 7.2, 150 mM NaCl) and incubated with 0.3 mM copper(II) sulfate (Acros Organics) and 0.3 mM 1,10-phenanthroline (Sigma-Aldrich) for 30 minutes. Cells were centrifuged (5,000 x g, 10 min, 4°C) and the pellets were frozen at −80°C prior to subsequent purification.

For the low resolution cryo-EM structure, the purification was performed similarly, but using plasmids pDT397 and pDT500 containing the S439C and E800C mutations, respectively. Cells were treated with BMOE as described above rather than with copper(II) sulfate and 1,10-phenanthroline.

Purification of substrate-bound Bam complex for cryo-EM.

Cell pellets expressing Bam-substrate complex as described above were thawed and resuspended in buffer containing 20 mM Tris-HCl pH 8.0, 150 mM NaCl, 100 μg/mL lysozyme (Sigma-Aldrich), 1 mM PMSF (Sigma-Aldrich), 50 μg/mL DNase I (Sigma-Aldrich), and 2.5 mM $MgCl_2$ (Sigma-Aldrich). Cells were lysed using an Emulsiflex C3 (Avestin) at a pressure of 10,000 to 15,000 psi. After lysis, cell debris was removed via centrifugation (5,000 x g, 10 min, 4°C). Membrane fractions were isolated via ultracentrifugation using a 45 Ti rotor (Beckman Coulter) (37,000 rpm, 45 min, 4°C) and an Optima XE-90 ultracentrifuge (Beckman Coulter). The membrane pellet was resuspended in buffer containing 20 mM Tris-HCl pH 8.0, 150 mM NaCl, 100 μg/mL lysozyme, and 1 mM PMSF. Membrane fractions were solubilized via incubation with 0.75% n-dodecyl-β-D-maltopyranoside (DDM, Anatrace) and 0.5% glyco-diosgenin (GDN, Anatrace) on a rocking

platform (2 hours, 4°C). Unsolubilized material was then isolated via ultracentrifugation in a 70 Ti rotor (Beckman Coulter) (37,000 rpm, 30 min, 4°C). The supernatant, consisting of solubilized membrane proteins, was removed and supplemented with imidazole (pH 8.0) to a final concentration of 5 mM.

The supernatant was incubated with Ni-nitrilotriacetic acid (NTA) resin (Qiagen) that had been pre-washed with 10 CV buffer W1 (20 mM Tris-HCl pH 8.0, 150 mM NaCl, 10 mM imidazole pH 8.0, 0.02% GDN). After batch binding on a rocking platform (1 hour, 4°C), the resin was washed with 10 CV buffer W1. Elution was performed via addition of 5 CV buffer E1 (20 mM Tris-HCl pH 8.0, 150 mM NaCl, 200 mM imidazole pH 8.0, 0.02% GDN).

The Ni-NTA eluate was immediately incubated with Strep-Tactin XT Superflow resin (IBA Lifesciences) that had been pre-washed with 10 CV buffer W2 (100 mM Tris-HCl pH 8.0, 150 mM NaCl, 0.02% GDN). After batch binding on a rocking platform (1 hour, 4°C), the resin was washed with 15 CV buffer W2. Elution was performed via addition of 9 CV buffer E2 (100 mM Tris-HCl pH 8.0, 150 mM NaCl, 1 mM EDTA, 50 mM D-biotin, 0.02% GDN).

The Strep resin eluate was concentrated using an Amicon Ultra 4 mL 100 kDa molecular-weight cutoff centrifugal concentrator (EMD Millipore). The sample was then applied to an ÄKTA Pure (GE Healthcare Life Sciences) for purification via size-exclusion chromatography using a Superdex 200 Increase 10/300 GL column. The protein was eluted in buffer containing 20 mM Tris-HCl pH 8.0, 150 mM NaCl, and 0.02% GDN. After elution, protein corresponding to the center peaks of the chromatogram was concentrated to 5 mg/mL using an Amicon Ultra 0.5 mL 100 kDa molecular-weight cutoff centrifugal concentrator (EMD Millipore). Regarding the purifications performed to obtain both the 4.1 Å and 6.5 Å structures, a final yield of approximately 0.1 mg of complex per liter of bacterial culture could be obtained.

Electron microscopy data collection.

Purified substrate-bound Bam complex as described above was applied to glow-discharged Quantifoil R 2/1 holey carbon 400-mesh copper grids (Quantifoil). Grids were blotted for 4–5 s at 100% humidity with the blot force set to 16, and flash frozen by liquid nitrogen-cooled liquid ethane using a Thermo Fisher Scientific Vitrobot Mark IV (Thermo Fisher Scientific). The grid was then loaded onto a Titan Krios G3i electron cryo-microscope (Thermo Fisher) operated at 300 kV accelerating voltage. Image stacks (movies) were recorded on a Gatan Bioquantum K3 Imaging Filter (Gatan, USA) using the super-resolution counting mode and the calibrated magnification of 58717× using SerialEM[49]. The slit of the energy filter was set to 25 eV, with a defocus range between 1.1 and 2.8 μm. The electron dose rate was 17 e−/physical pixel per second, and the subframe time was set to 0.06 second. A total exposure time of 3 second resulted in 50 subframes per image stack. The total electron dose was 70 e−/Å^2 (~1.4 e−/Å^2 per subframe). The multi-shot scheme in SerialEM was used for data collection, with settings of 4 holes per stage move, and 5 shots per hole, which greatly sped up the data collection. The data collection for both structures (4.1 Å and 6.5 Å) was performed in the same manner.

Image processing and 3D reconstruction.

The movie frames were motion-corrected and dose-weighted by MotionCor2[50] and CTF parameters were estimated by CTFFIND4[51]. Particle picking was carried out using crYOLO[52] giving 2,054,956 initial particles. Following successive rounds of 2D and 3D classification within Relion[53], 516,419 particles were then "polished" through the Bayesian polishing process[54]. These particles were then subjected to further 2D and 3D classification within CryoSPARC[55], after which 223,353 particles were selected (see classification flowchart in Extended Data Figure 3) and subjected to non-uniform refinement in CryoSPARC, which led to the final reconstruction at 4.1 Å resolution. Masking strategies did not yield an improved structure. Maps used for figures were filtered according to local resolution with B-factor sharpening within CryoSPARC.

For the low resolution (6.5 Å) structure, the movie frames were motion-corrected and dose-weighted by MotionCor2[50] and CTF parameters were estimated by CTFFIND4[51]. Particle picking was carried out using crYOLO[52] giving 690,143 initial particles. Following successive rounds of 2D and 3D classification within Relion[53], 233,064 particles were then "polished" through the Bayesian polishing process[54]. Refinement in Relion led to the final reconstruction at 6.5 Å resolution. Masking strategies did not yield an improved structure. Maps used for figures were filtered according to local resolution with b-factor sharpening within Relion. Structural biology applications used in this project (other than CryoSPARC) were compiled and configured by SBGrid[56].

Model building, refinement, and validation.

The atomic model was generated using available structures of the Bam complex components. For $BamA^{M}BDE$, an initial model was generated by rigid-body fitting these components into the 4.1 Å EM map using UCSF Chimera[57]. The $BamA^{M}$ POTRA domains and BamE were obtained from PDB ID: 5D0O. The $BamA^{M}$ β-barrel and BamD were obtained from PDB ID: 5D0Q. BamB was obtained from PDB ID: 2YH3. For the substrate, a homology model generated with I-TASSER was used[58–60].

The initial modeling was followed by manual adjustments using Coot[61]. All selenomethiones were replaced with methionines. The improved model was then refined in real space against the cryo-EM map using real space refinement in PHENIX[62] with secondary structure restraints. Iterative rounds of manual and automated refinement in Coot and PHENIX, respectively, generated a model that included all components except for BamC and the POTRA domains 1 and 2 of $BamA^{M}$. Due to the lower resolution of these components, the atomic models were generated by docking previously determined structures into our map (from 5D0Q for BamC and 5D0O for the POTRA domains) without further refinement. For the entirety of POTRA domains 1 and 2 of $BamA^{M}$ (residues 1–171) and the C-terminal domain of BamC (residues 89–209), only the main chain atoms are included in the model. For the substrate, the two POTRA domains could not be resolved, so they are not included in the model. The final model was visually inspected for general fit to the map, and geometry was further evaluated using MolProbity[63]. Cryo-EM data collection, refinement, and validation statistics are summarized in Supplementary Table 1. Figures depicting the structure were prepared in Chimera or PyMOL (Schrödinger, https://www.pymol.org).

Extended Data

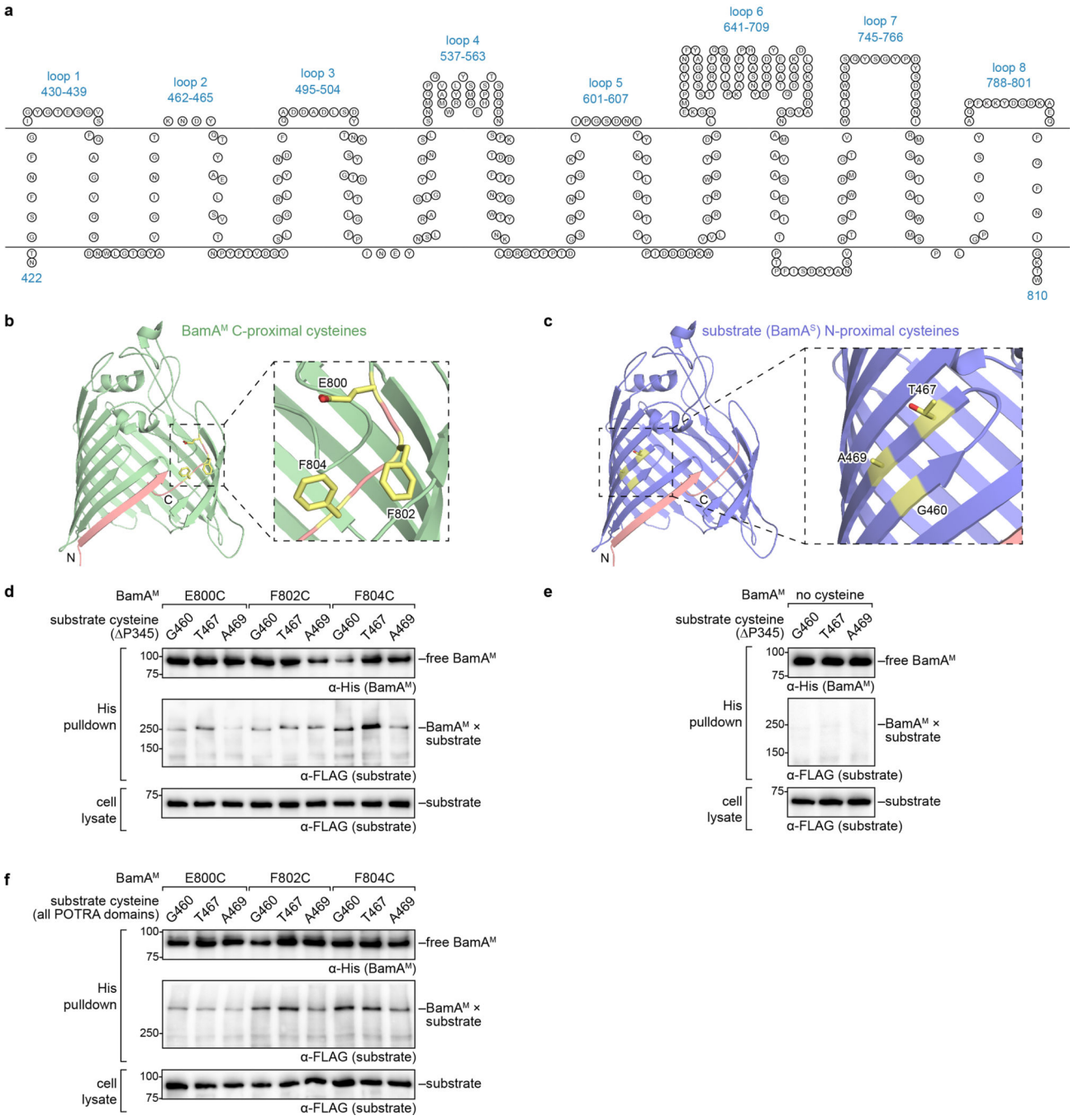

Extended Data Figure 1 |. Capturing the BamA^S-ΔL1 substrate on the Bam complex using disulfide bond formation.

a, Topological map of the β-barrel domain of BamA with extracellular loops labelled. **b**, Residues near the C-terminus of the β-barrel domain of BamA^M that were substituted with cysteine (yellow sticks) shown on the structure of the β-barrel domain of BamA (green, PDB ID: 5D0O). The N- and C-terminal β-strands are labelled and shown in salmon. **c**, As in **b**, but showing residues near the N-terminus of the β-barrel domain of the substrate (BamA^S-ΔL1, blue) that were substituted with cysteine. The positions of these cysteine substitutions

were selected based on reports that the C-terminal region of $BamA^{M}$ is in proximity to the N-terminal region of the substrate during folding[10–12]. **d**, Disulfide bond formation between 6×His-tagged $BamA^{M}$ and 3×FLAG-tagged $BamA^{S}$-ΔP345-ΔL1 containing cysteine substitutions shown in **b** and **c**. The presence of a Bam-substrate disulfide bond is detected as a high molecular weight adduct on the α-FLAG (middle) immunoblot. The adducts generated via disulfide bond formation were not present in an amount high enough for detection with the α-His antibody but could be detected with the α-FLAG antibody. α-FLAG immunoblot of total cell lysates (bottom) shows that the substrates containing different cysteine substitutions are expressed at similar levels. In this experiment, no oxidizing agent (e.g., copper(II) sulfate and 1,10-phenanthroline) was added. **e**, As in **d**, but without any cysteine introduced into $BamA^{M}$. Disulfide bond formation is not observed between $BamA^{M}$ and the substrates when no cysteine is introduced into $BamA^{M}$. **f**, As in **d**, but with substrates containing all five POTRA domains. Disulfide bond formation between $BamA^{M}$ and substrates containing all POTRA domains indicates that stalling of substrates in **d** is not due to deletion of POTRA domains 3–5. Data shown in **d-f** are representative of results from two biological replicates.

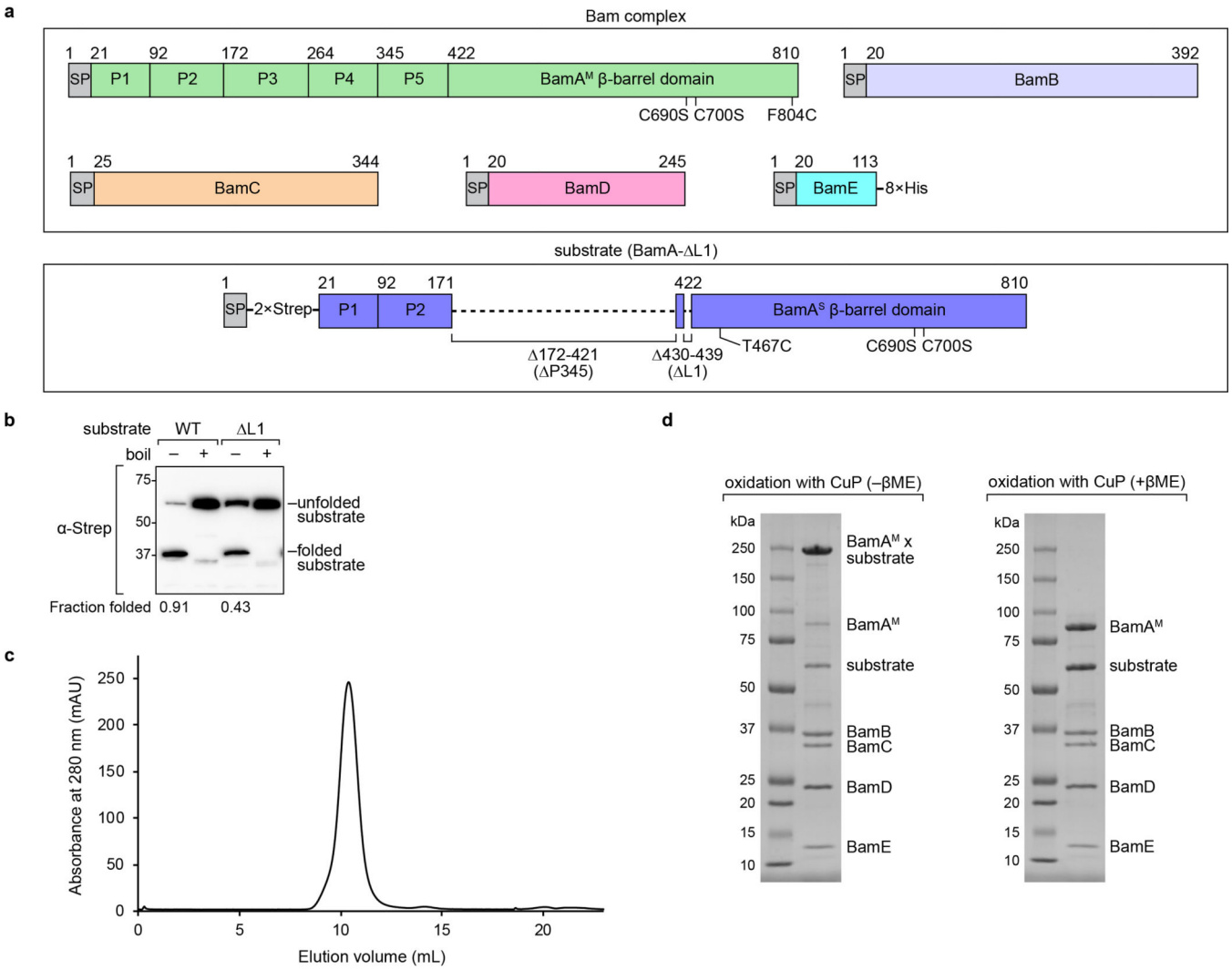

Extended Data Figure 2 |. Expression and purification of substrate-bound Bam complex for cryo-EM.

a, Constructs used for protein expression. Mutations and affinity tags introduced into each protein are indicated. SP represents signal peptide; P1 to P5 represent the POTRA domains of BamA. The substrates also contain deletion of POTRA domains 3, 4, and 5 (Δ172–421) to avoid the possibility of these substrates forming Bam complexes if they complete folding. The deletion does not prevent folding of an otherwise wild-type BamA (see below). **b**, Assessment of heat modifiability of substrate used for cryo-EM (ΔL1, right half of blot) that contains the T467C mutation and a substrate that contains loop 1 but is otherwise identical (WT, left half of blot). The samples in the unboiled lanes can be used to calculate the fraction of each substrate that is folded *in vivo* (indicated below the blot). $BamA^S$-ΔL1 accumulates on the Bam complex because of the deletion of loop 1. **c**, Representative size-exclusion chromatogram of the substrate-bound Bam complex in which disulfide bond formation between the N-terminus of the substrate ($BamA^S$-ΔL1) and the C-terminus of $BamA^M$ was induced with the oxidizing agent copper sulfate/1,10-phenanthroline (CuP). **d**, SDS-PAGE gels showing peak fractions from size-exclusion chromatography of the complex

in **c**. The left gel shows the complex without addition of βME, while the right gel shows the complex after addition of βME to break the disulfide bond. Data shown in **b**-**d** are representative of results from two biological replicates.

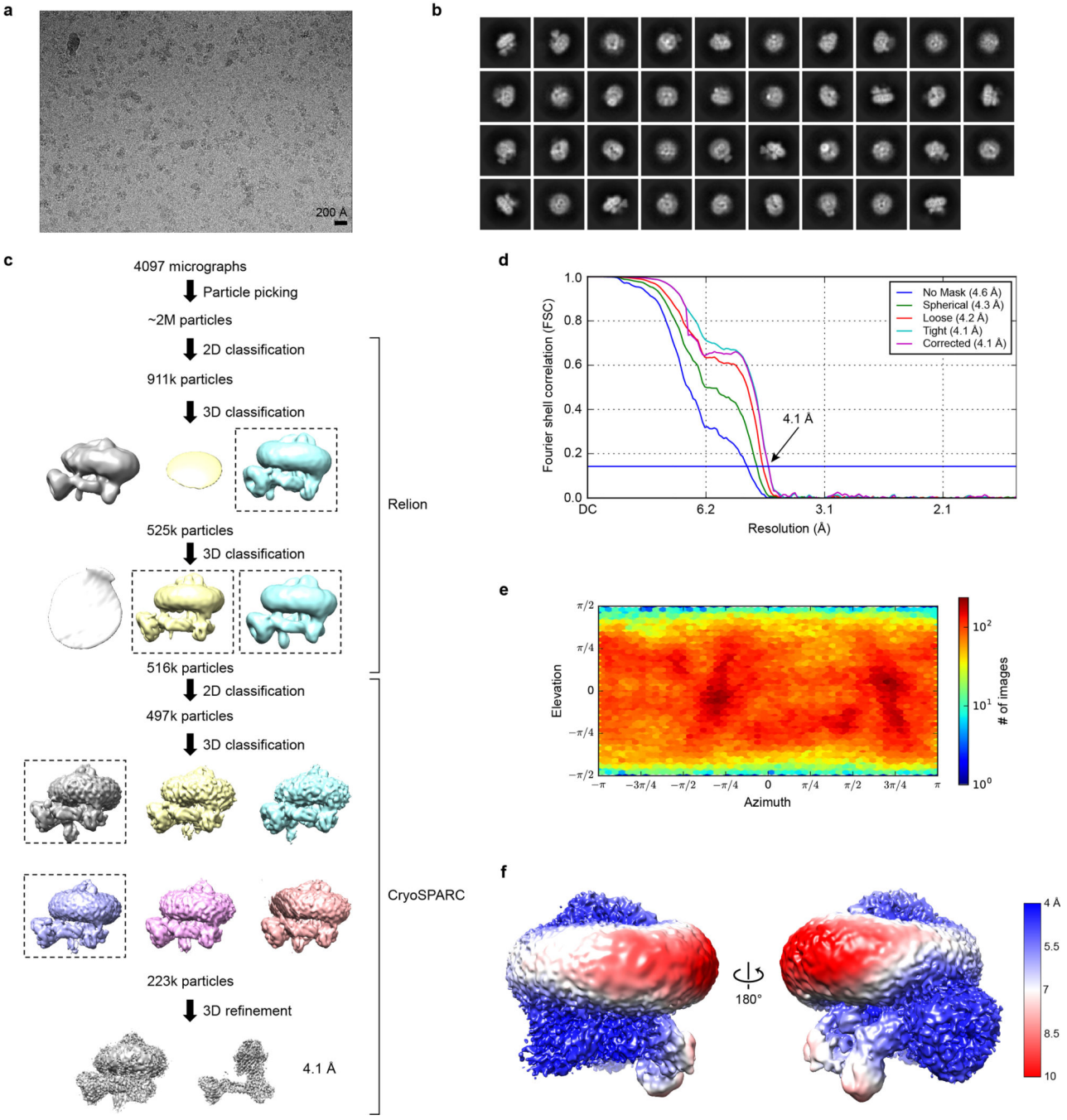

Extended Data Figure 3 |. Cryo-EM data processing and analysis for substrate-bound Bam complex.

a, Representative cryo-EM micrograph of the substrate-bound Bam complex embedded in vitreous ice. **b**, Selected two-dimensional class averages of cryo-EM particle images. **c**, Scheme of three-dimensional classification and refinement of cryo-EM particle images. **d**, Gold-standard Fourier shell correlation (FSC) curves calculated with different masks in cryoSPARC. The resolutions were determined at FSC = 0.143 (horizontal blue line). The final corrected mask gave an overall resolution of 4.1 Å. **e**, Distribution of orientations over

azimuth and elevation angles for particles included in the calculation of the final map. **f**, Cryo-EM map colored by local resolution as shown in Figure 1g, but at a lower contour level.

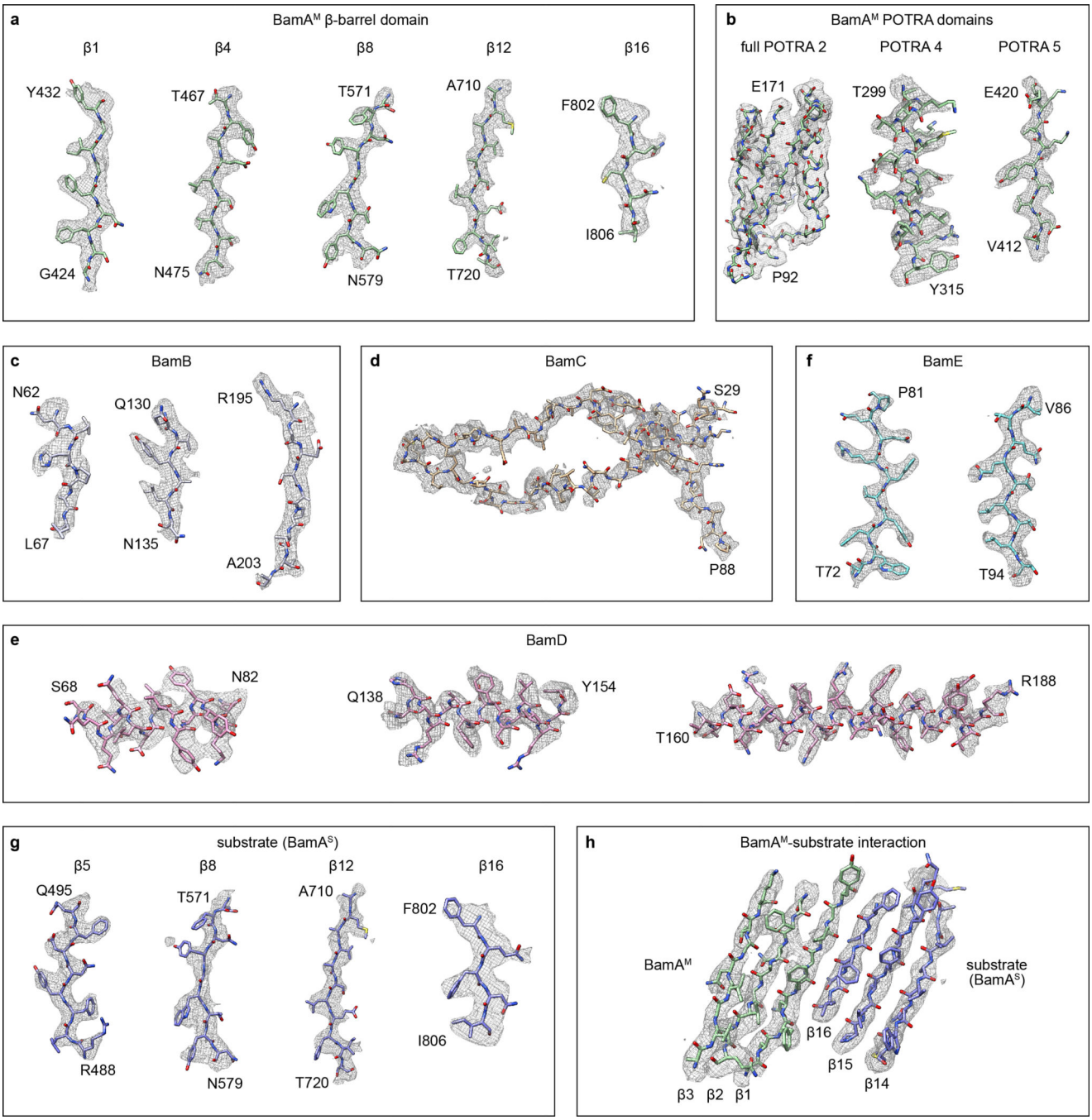

Extended Data Figure 4 |. Fit of the atomic model into the cryo-EM map.

The atomic model (in stick representation) shown with the corresponding portion of the cryo-EM map (shown in gray mesh) for selected regions in **a**, the $BamA^{M}$ β-barrel domain; **b**, the $BamA^{M}$ POTRA domains; **c**, BamB; **d**, BamC; **e**, BamD; **f**, BamE; **g**, the substrate; and **h**, the $BamA^{M}$-substrate interaction. Side-chain densities are visible, and individual β-strands can be resolved. Images were prepared in UCSF Chimera using a 2 Å carve radius.

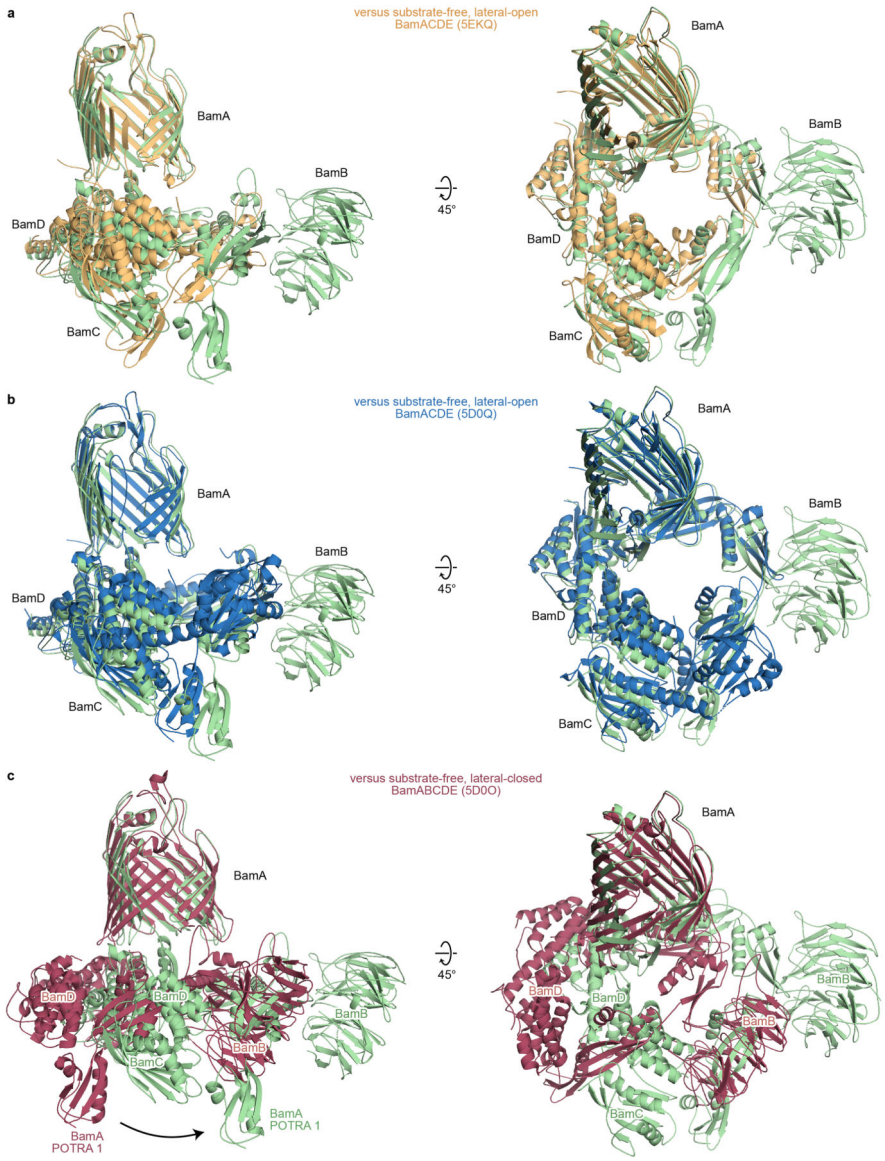

Extended Data Figure 5 |. Comparison of the architecture of the substrate-bound Bam complex to that of substrate-free Bam complexes.

a-c, Alignments of substrate-bound Bam complex (all components shown in green) with published Bam complex structures (shown in different colors). Alignments are performed using the β-barrel domains of BamA.

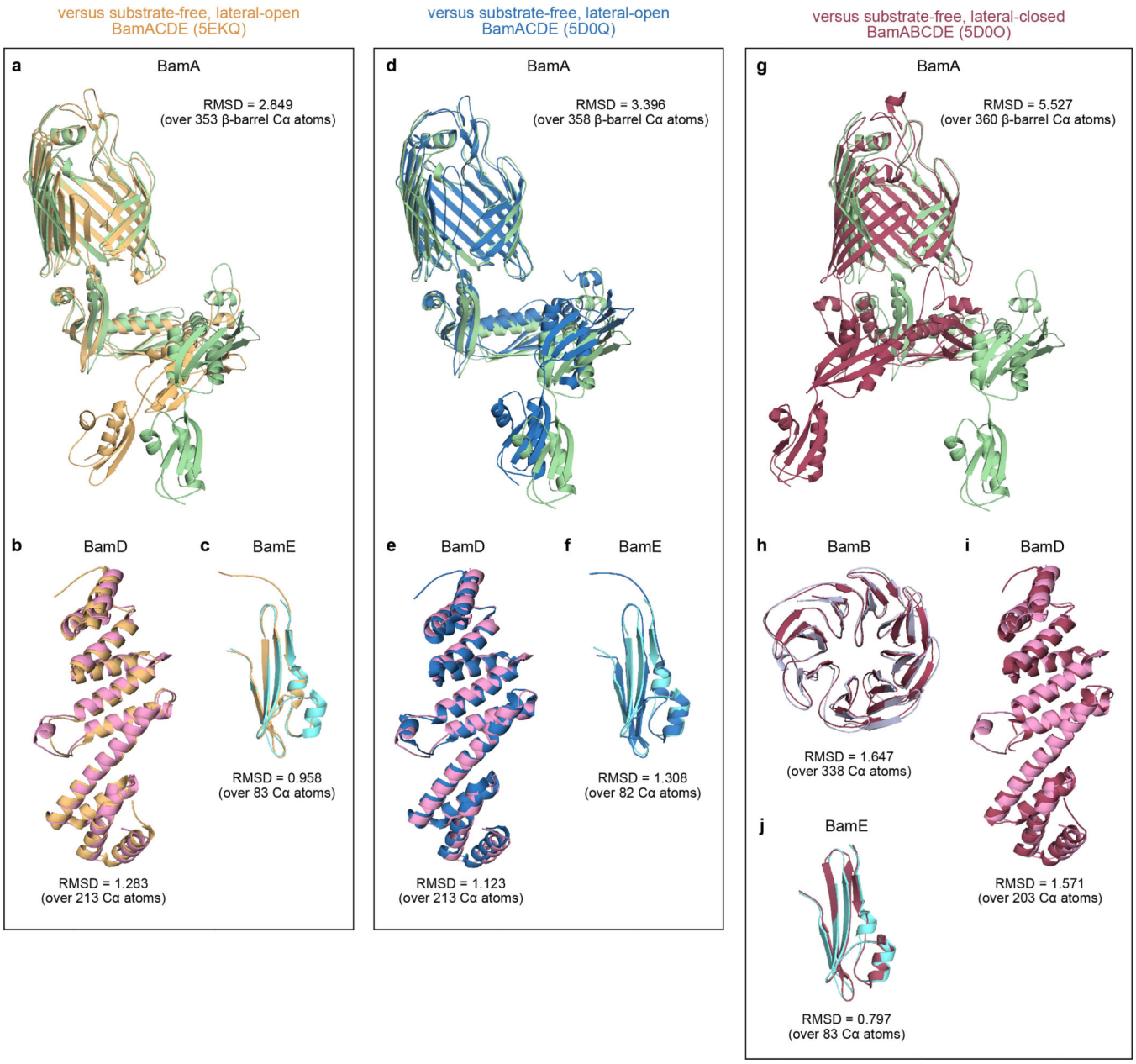

Extended Data Figure 6 |. Conformational differences between Bam complex components from substrate-bound and substrate-free complexes.

Alignments of atomic models of **a**, $BamA^{M}$; **b**, BamD; and **c**, BamE from our substrate-bound complex (colored as in Figure 2) with the corresponding components from a substrate-free, lateral-open Bam complex (light orange, PDB ID: 5EKQ). **d**-**f**, as in **a**-**c**, but using a different substrate-free, lateral-open Bam complex (blue, PDB ID: 5D0Q). Alignments of atomic models of **g**, $BamA^{M}$; **h**, BamB; **i**, BamD; and **j**, BamE from our substrate-bound complex with the corresponding components from a substrate-free, lateral-closed Bam complex (dark red, PDB ID: 5D0O). Alignments of $BamA^{M}$ are performed using the β-barrel domains. Alignments of BamB are not shown for complexes in which BamB is absent. Alignments of BamC are not shown since BamC in our structure was

obtained by docking BamC as a rigid body from PDB ID: 5D0Q. The RMSD value for each alignment, obtained with PyMOL, is indicated.

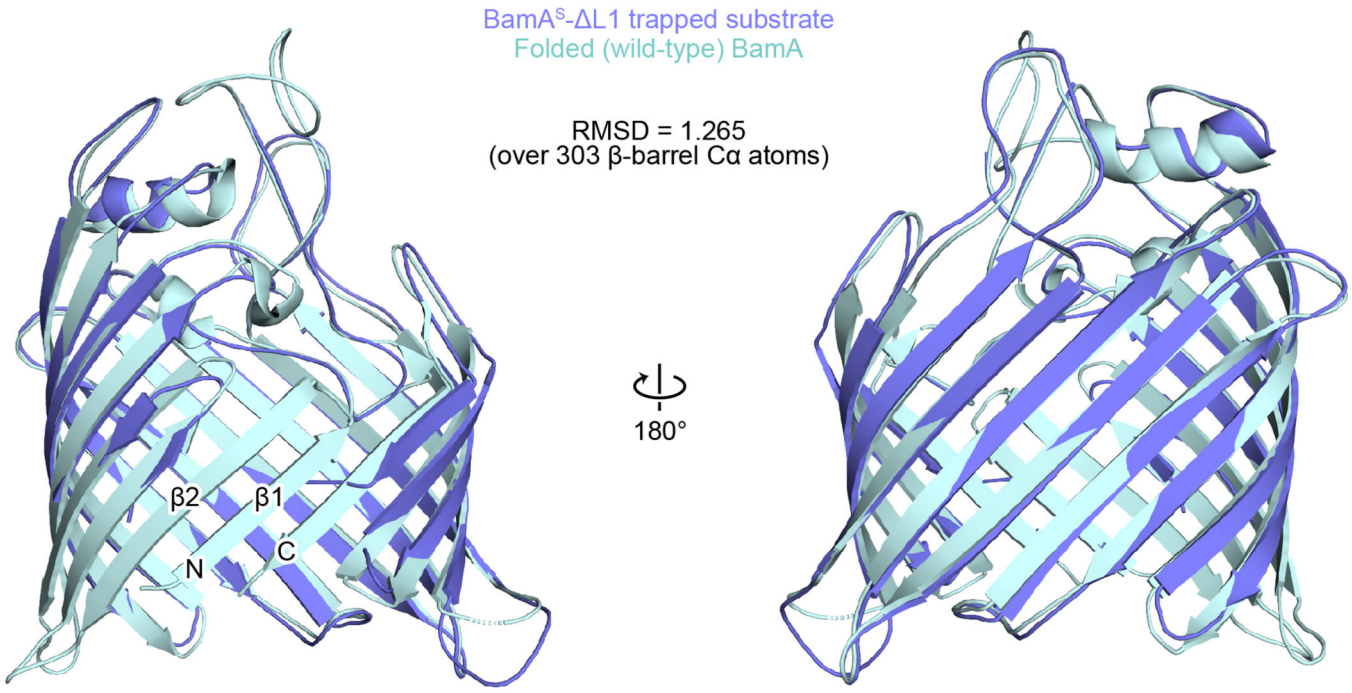

Extended Data Figure 7 |. The BamA^S-ΔL1 substrate accumulates on the Bam complex in a largely folded state.

Alignment of the atomic model of the BamA^S-ΔL1 substrate (blue) with that of folded wild-type BamA (cyan, PDB ID: 4N75). The first two β-strands of the substrate in our structure could not be resolved (β1 and β2, labelled on the structure of wild-type BamA). The similarity between the trapped substrate and folded wild-type BamA suggests that the former represents an on-pathway folding intermediate.

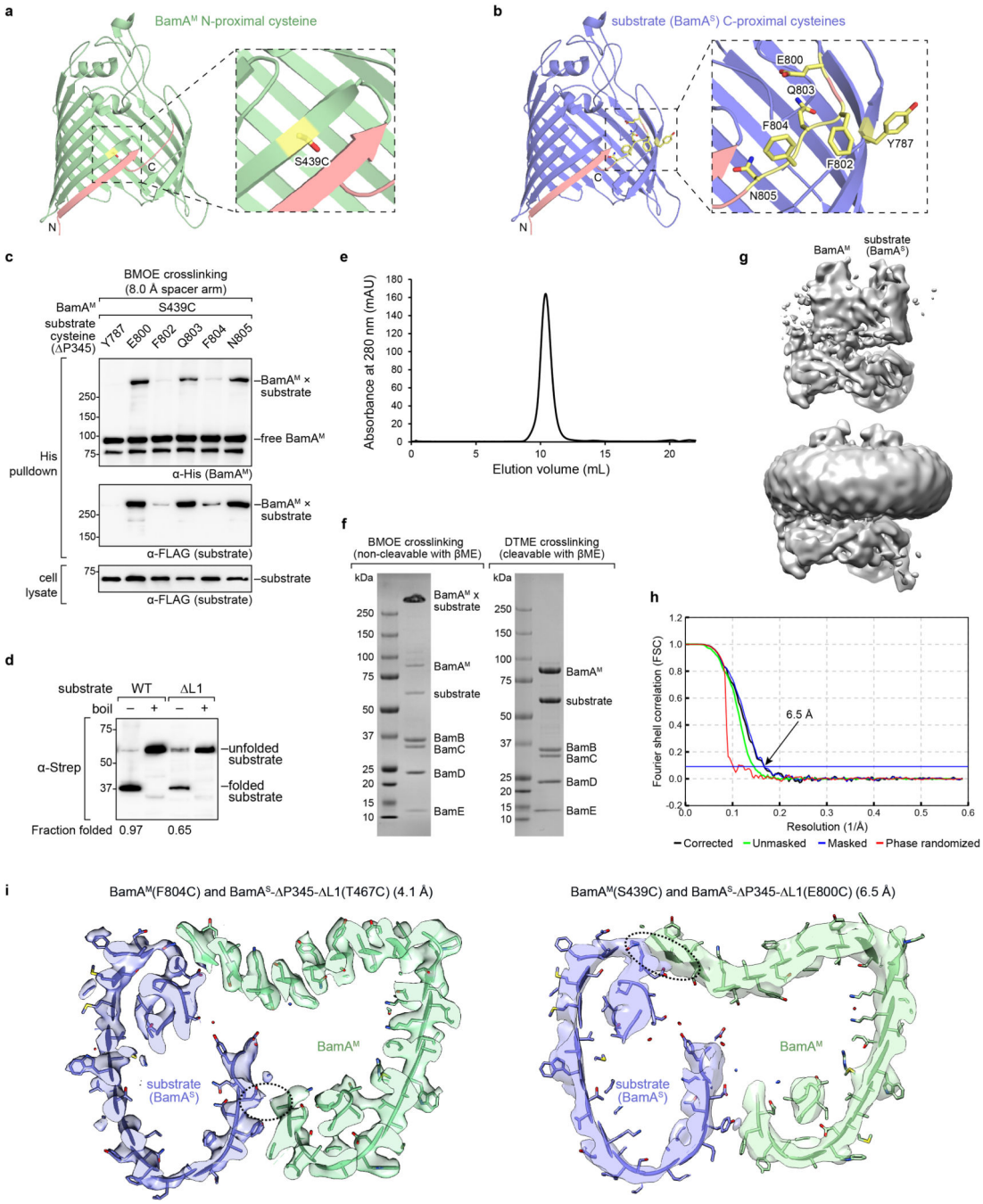

Extended Data Figure 8 |. Low resolution cryo-EM structure of a substrate-bound Bam complex with an alternative cysteine crosslink.

a, Residue near the N-terminus of the β-barrel domain of $BamA^M$ that was substituted with cysteine (yellow stick) shown on the structure of the β-barrel domain of BamA (green, PDB ID: 5D0O). The N- and C-terminal β-strands are labelled and shown in salmon. **b**, As in **a**, but showing residues near the C-terminus of the β-barrel domain of the substrate ($BamA^S$-ΔL1, blue) that were substituted with cysteine. **c**, Cysteine crosslinking between 6×His-tagged $BamA^M$ and 3×FLAG-tagged $BamA^S$-ΔP345-ΔL1 containing cysteine substitutions

shown in **a** and **b**. The crosslinker 1,2-bis(maleimido)ethane (BMOE), which has an 8.0 Å spacer arm, was used. The presence of a Bam-substrate crosslink is detected as a high molecular weight adduct on α-His (top) and α-FLAG (middle) immunoblots. α-FLAG immunoblot of total cell lysates (bottom) shows that the substrates containing different cysteine substitutions are expressed at similar levels. Based on these results, E800C was selected for use within $BamA^{S}$-ΔL1 for cryo-EM, while S439C was introduced into $BamA^{M}$. **d**, Assessment of heat modifiability of substrate used for cryo-EM (ΔL1, right half of blot) that contains the E800C mutation and a substrate that contains loop 1 but is otherwise identical (WT, left half of blot). The samples in the unboiled lanes can be used to calculate the fraction of each substrate that is folded *in vivo* (indicated below the blot). The substrate containing the E800C mutation retains the ability to fold *in vivo*. **e**, Representative size-exclusion chromatogram of the substrate-bound Bam complex in which cysteine crosslink formation between the C-terminus of the substrate ($BamA^{S}$-ΔL1) and the N-terminus of $BamA^{M}$ was induced with BMOE. **f**, SDS-PAGE gels showing peak fractions from size-exclusion chromatography. The left gel shows the complex from **e** with addition of βME, which cannot break the crosslink formed by BMOE. The right gel shows the complex crosslinked with dithiobismaleimidoethane (DTME), which is similar to BMOE, but has a 13.3 Å spacer arm and is cleavable in the presence of βME to visualize the individual components of the complex. **g**, Cryo-EM map obtained using the $BamA^{M}$(S439C) and $BamA^{S}$-ΔP345-ΔL1(E800C) cysteine pair crosslinked with BMOE. The two images show the same view at different contour levels. $BamA^{M}$ and the substrate are labelled. **h**, Gold-standard Fourier shell correlation (FSC) curves for low resolution cryo-EM structure calculated in Relion. The final corrected mask gave an overall resolution of 6.5 Å at FSC = 0.143 (horizontal blue line). **i**, Comparison of the 4.1 Å structure to the 6.5 Å structure containing the alternative cysteine pair in $BamA^{M}$ and the substrate. In the left panel, a top-down slice through the 4.1 Å cryo-EM map is shown (similar to the slice in Fig. 3c) and is overlaid with the atomic model generated from that map. In the right panel, a similar slice through the 6.5 Å cryo-EM map is shown and is overlaid with the atomic model generated from the 4.1 Å map after fitting of the atomic model into the 6.5 Å map as a rigid body. The dashed oval represents the approximate location of the cysteine tether introduced into each complex. The use of different cysteine pairs yielded similar cryo-EM structures, showing that the presence of the disulfide bond in the main (4.1 Å) structure did not introduce a non-native conformation into the complex. Data shown in **c**-**f** are representative of results from two biological replicates.

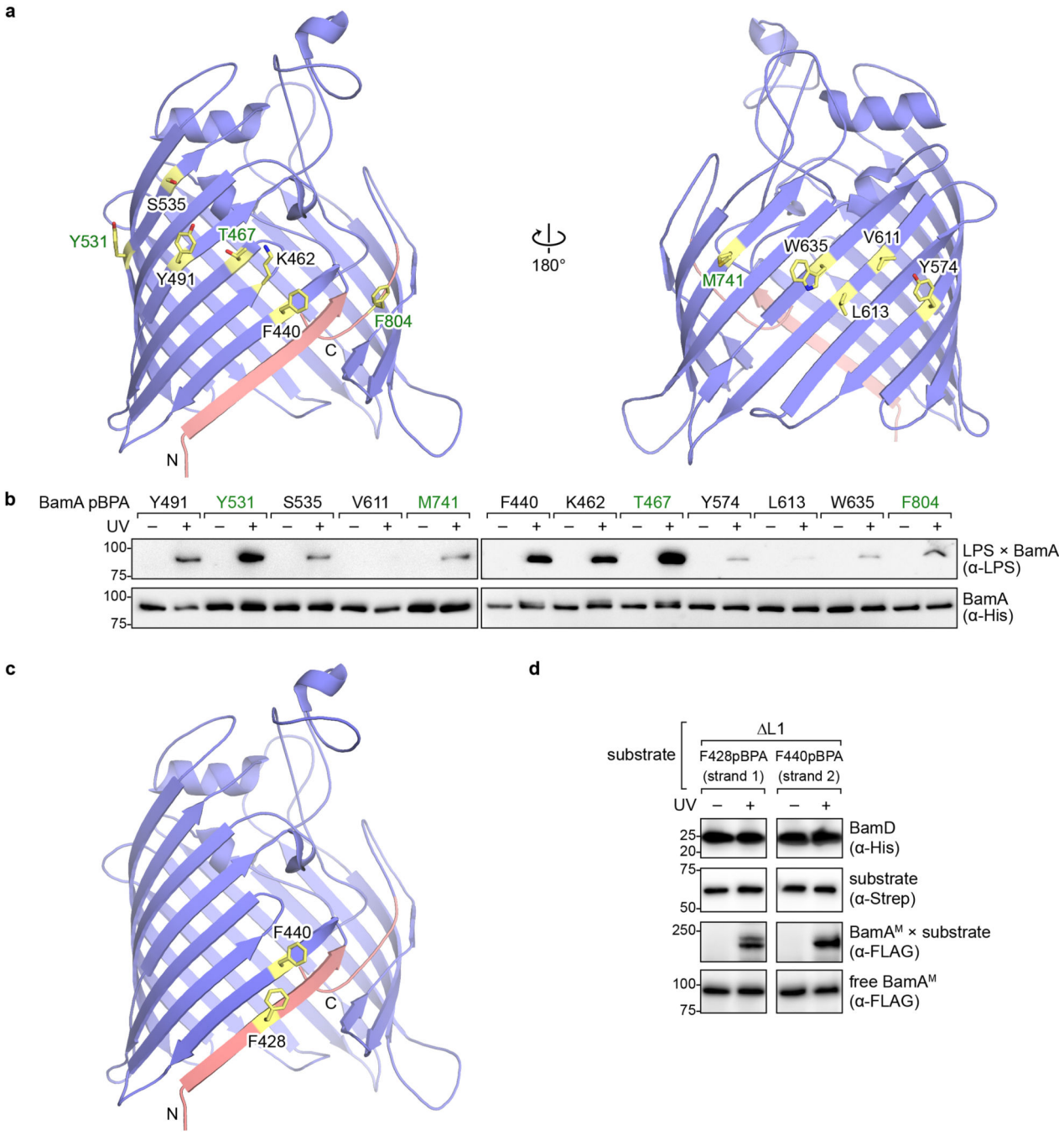

Extended Data Figure 9 |. *In vivo* photocrosslinking with wild-type BamA and BamA^{S}-ΔL1.
a, Residues in BamA substituted with the photocrosslinkable amino acid pBPA (yellow sticks) shown on the structure of the β-barrel domain of BamA (blue, PDB ID: 5D0O). These pBPA substitutions were used to observe crosslinks to LPS. The N- and C-termini of BamA are shown in salmon. All highlighted residues have side chains oriented outward towards the membrane environment. **b**, *In vivo* photocrosslinking of BamA to LPS. In **a** and **b**, the pBPA substitutions that were subsequently used to test crosslinking of stalled substrates to LPS (in Figure 3d) are indicated in green. **c**, Residues in β-strands 1 and 2 of

BamA^{S}-ΔL1 substituted with pBPA shown on the structure of the β-barrel domain of BamA. Colors are as described in **a**. These positions were selected since β-strands 1 and 2 of the substrate are not visible in the cryo-EM structure (Extended Data Figure 8). **d**, *In vivo* photocrosslinking of Strep-tagged BamA^{S}-ΔL1 containing pBPA at positions F428 or F440 and deletion of POTRA domains 3–5. Immunoblotting was performed using α-His, α-Strep, and α-FLAG antibodies to detect BamD (loading control), BamA^{S}-ΔL1, and BamA^{M}, respectively. For α-FLAG immunoblot, a longer exposure (top, to detect crosslinks) and a shorter exposure (bottom) are shown. Although β-strands 1 and 2 of the substrate are not visible in the cryo-EM structure, the *in vivo* photocrosslinking results show that residues within these β-strands are in proximity to BamA^{M}. The experiment in **b** was performed once, and the pBPA substitutions indicated in green were tested again in Figure 3d. Data shown in **d** are representative of results from two biological replicates.

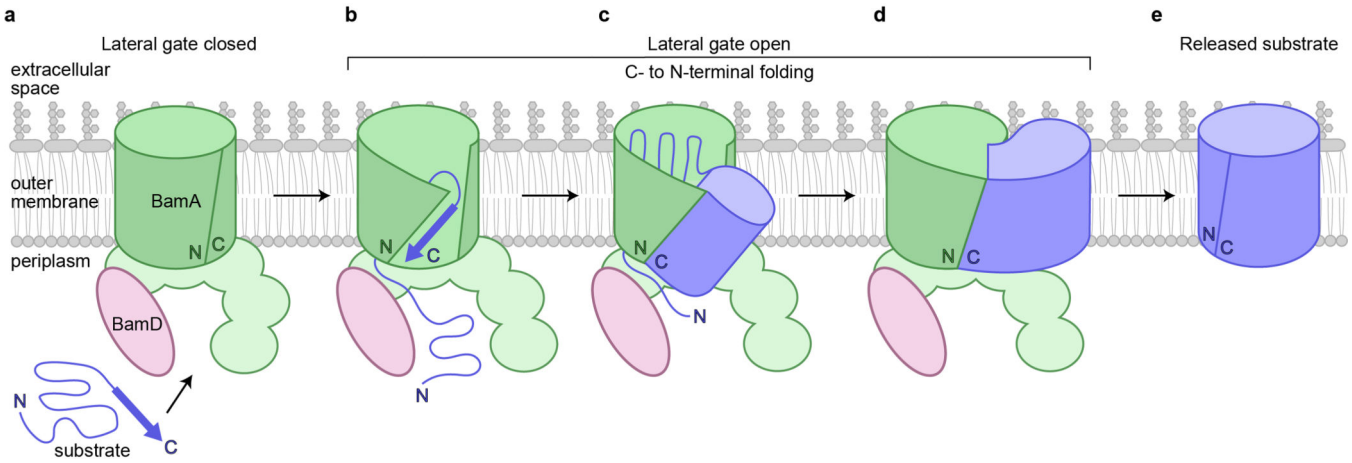

Extended Data Figure 10 |. Proposed model of β-barrel assembly by the Bam complex.

a, The substrate is recruited to the Bam complex. $BamA^{M}$ is in a closed state prior to substrate-induced opening of its lateral gate. For simplicity, only $BamA^{M}$, the substrate, and BamD are shown. **b-d**, The C-terminus of the substrate interacts with the exposed N-terminal edge of $BamA^{M}$, and β-strands or β-hairpins of the substrate are added sequentially from the C- to N-terminus. Early folding may occur within the interior of the $BamA^{M}$ β-barrel[12], and folded portions of the substrate may then be released outward. Full membrane integration could occur after a substantial amount of folding. Steps **b** and **c** represent intermediate stages to **d**, which corresponds to the cryo-EM structure of the substrate-bound Bam complex. **e**, The substrate is released into the membrane environment once its N- and C-terminal ends are joined.

Supplementary Material

Refer to Web version on PubMed Central for supplementary material.

Acknowledgements:

We thank Sarah Sterling, Richard Walsh, and Melissa Chambers at the Harvard Cryo-EM Center for Structural Biology for assistance with electron microscopy; Richard Losick, Suzanne Walker, Andrew Kruse, Mary May, Karanbir Pahil, Rebecca Taylor, and Michael Mandler for providing feedback on the manuscript; and Harris Bernstein (NIH) for the kind gift of the pJH114 plasmid. This work was supported by NIH grants F31GM116210 (to J.L.), F32GM108258 (to J.S.W.), and R01GM066174 and R01AI081059 (to D.K.). S.C.H. is an Investigator in the Howard Hughes Medical Institute.

References

1. Walther DM, Rapaport D. & Tommassen J. Biogenesis of β-barrel membrane proteins in bacteria and eukaryotes: Evolutionary conservation and divergence. Cellular and Molecular Life Sciences (2009). doi:10.1007/s00018-009-0029-z
2. Hagan CL, Silhavy TJ & Kahne D. β-Barrel membrane protein assembly by the Bam complex. Annu. Rev. Biochem 80, 189–210 (2011). [PubMed: 21370981]
3. Paschen SA et al. Evolutionary conservation of biogenesis of beta-barrel membrane proteins. Nature 426, 862–866 (2003). [PubMed: 14685243]
4. Wiedemann N. et al. Machinery for protein sorting and assembly in the mitochondrial outer membrane. Nature 424, 565–571 (2003). [PubMed: 12891361]

5. Wu T. et al. Identification of a multicomponent complex required for outer membrane biogenesis in Escherichia coli. Cell 121, 235–245 (2005). [PubMed: 15851030]
6. Voulhoux R, Bos MP, Geurtsen J, Mols M. & Tommassen J. Role of a highly conserved bacterial protein in outer membrane protein assembly. Science 299, 262–5 (2003). [PubMed: 12522254]
7. Malinverni JC et al. YfiO stabilizes the YaeT complex and is essential for outer membrane protein assembly in Escherichia coli. Mol. Microbiol 61, 151–164 (2006). [PubMed: 16824102]
8. Sklar JG et al. Lipoprotein SmpA is a component of the YaeT complex that assembles outer membrane proteins in Escherichia coli. Proc. Natl. Acad. Sci. U. S. A 104, 6400–6405 (2007). [PubMed: 17404237]
9. Hagan CL, Kim S. & Kahne D. Reconstitution of outer membrane protein assembly from purified components. Science 328, 890–892 (2010). [PubMed: 20378773]
10. Höhr AIC et al. Membrane protein insertion through a mitochondrial β-barrel gate. Science (80-.) 359, eaah6834 (2018).
11. Doyle MT & Bernstein HD Bacterial outer membrane proteins assemble via asymmetric interactions with the BamA β-barrel. Nat. Commun (2019). doi:10.1038/s41467-019-11230-9
12. Lee J. et al. Formation of a β-barrel membrane protein is catalyzed by the interior surface of the assembly machine protein BamA. Elife 8, (2019).
13. Noinaj N. et al. Structural insight into the biogenesis of β-barrel membrane proteins. Nature (2013). doi:10.1038/nature12521
14. Bakelar J, Buchanan SK & Noinaj N. The structure of the β-barrel assembly machinery complex. Science (80-.) 351, 180–186 (2016).
15. Gu Y. et al. Structural basis of outer membrane protein insertion by the BAM complex. Nature (2016). doi:10.1038/nature17199
16. Han L. et al. Structure of the BAM complex and its implications for biogenesis of outer-membrane proteins. Nat. Struct. Mol. Biol (2016). doi:10.1038/nsmb.3181
17. Iadanza MG et al. Lateral opening in the intact β-barrel assembly machinery captured by cryo-EM. Nat. Commun 7, 12865 (2016). [PubMed: 27686148]
18. Kim KH, Aulakh S. & Paetzel M. The bacterial outer membrane β-barrel assembly machinery. Protein Science (2012). doi:10.1002/pro.2069
19. Noinaj N, Kuszak AJ, Balusek C, Gumbart JC & Buchanan SK Lateral opening and exit pore formation are required for BamA function. Structure (2014). doi:10.1016/j.str.2014.05.008
20. Schiffrin B, Brockwell DJ & Radford SE Outer membrane protein folding from an energy landscape perspective. BMC Biology (2017). doi:10.1186/s12915-017-0464-5
21. Hagan CL & Kahne D. The reconstituted Escherichia coli Bam complex catalyzes multiple rounds of β-barrel assembly. Biochemistry 50, 7444–7446 (2011). [PubMed: 21823654]
22. Plummer AM & Fleming KG BamA Alone Accelerates Outer Membrane Protein Folding in Vitro through a Catalytic Mechanism. Biochemistry (2015). doi:10.1021/acs.biochem.5b00950
23. Wzorek JS, Lee J, Tomasek D, Hagan CL & Kahne DE Membrane integration of an essential β-barrel protein prerequires burial of an extracellular loop. Proc. Natl. Acad. Sci 114, 2598–2603 (2017). [PubMed: 28223520]
24. Hagan CL, Westwood DB & Kahne D. Bam Lipoproteins Assemble BamA in Vitro. Biochemistry 52, 6108–6113 (2013). [PubMed: 23919461]
25. Gu Y, Zeng Y, Wang Z. & Dong C. BamA β16C strand and periplasmic turns are critical for outer membrane protein insertion and assembly. Biochem. J (2017). doi:10.1042/BCJ20170636
26. Browning DF et al. Mutational and topological analysis of the Escherichia coli BamA protein. PLoS One (2013). doi:10.1371/journal.pone.0084512
27. Albrecht R. & Zeth K. Structural basis of outer membrane protein biogenesis in bacteria. J. Biol. Chem (2011). doi:10.1074/jbc.M111.238931
28. Lee J. et al. Characterization of a stalled complex on the β-barrel assembly machine. Proc. Natl. Acad. Sci 113, 8717–8722 (2016). [PubMed: 27439868]
29. Sikdar R, Peterson JH, Anderson DE & Bernstein HD Folding of a bacterial integral outer membrane protein is initiated in the periplasm. Nat. Commun (2017). doi:10.1038/s41467-017-01246-4

30. Harrison SC Peptide-surface association: The case of PDZ and PTB domains. Cell (1996). doi:10.1016/S0092-8674(00)80105-1
31. Remaut H. & Waksman G. Protein-protein interaction through β-strand addition. Trends in Biochemical Sciences (2006). doi:10.1016/j.tibs.2006.06.007
32. Kim S. et al. Structure and function of an essential component of the outer membrane protein assembly machine. Science 317, 961–964 (2007). [PubMed: 17702946]
33. White SH & Wimley WC Membrane protein folding and stability: Physical principles. Annu. Rev. Biophys. Biomol. Struct (1999). doi:10.1146/annurev.biophys.28.1.319
34. Roseman MA Hydrophobicity of the peptide CO···HN hydrogen-bonded group. J. Mol. Biol (1988). doi:10.1016/0022-2836(88)90642-0
35. Ni D. et al. Structural and functional analysis of the β-barrel domain of BamA from Escherichia coli. FASEB J. (2014). doi:10.1096/fj.13-248450
36. Lundquist K, Bakelar J, Noinaj N. & Gumbart JC C-terminal kink formation is required for lateral gating in BamA. Proc. Natl. Acad. Sci (2018). doi:10.1073/pnas.1722530115
37. Storek KM et al. Monoclonal antibody targeting the β-barrel assembly machine of Escherichia coli is bactericidal. Proc. Natl. Acad. Sci. U. S. A (2018). doi:10.1073/pnas.1800043115
38. Hart EM et al. A small-molecule inhibitor of BamA impervious to efflux and the outer membrane permeability barrier. Proc. Natl. Acad. Sci. U. S. A (2019). doi:10.1073/pnas.1912345116
39. Luther A. et al. Chimeric peptidomimetic antibiotics against Gram-negative bacteria. Nature (2019). doi:10.1038/s41586-019-1665-6
40. Imai Y. et al. A new antibiotic selectively kills Gram-negative pathogens. Nature (2019). doi:10.1038/s41586-019-1791-1

Supplementary References

41. Casadaban MJ Transposition and fusion of the lac genes to selected promoters in Escherichia coli using bacteriophage lambda and Mu. J. Mol. Biol (1976). doi:10.1016/0022-2836(76)90119–4
42. Leo JC, Oberhettinger P. & Linke D. Assessing the Outer Membrane Insertion and Folding of Multimeric Transmembrane β-Barrel Proteins. Methods Mol. Biol 1329, 157–67 (2015). [PubMed: 26427683]
43. Villa R. et al. The Escherichia coli Lpt transenvelope protein complex for lipopolysaccharide export is assembled via conserved structurally homologous domains. J. Bacteriol 195, 1100–8 (2013). [PubMed: 23292770]
44. Freinkman E, Chng S-S & Kahne D. The complex that inserts lipopolysaccharide into the bacterial outer membrane forms a two-protein plug-and-barrel. Proc. Natl. Acad. Sci. U. S. A 108, 2486–91 (2011). [PubMed: 21257904]
45. Hagan CL, Wzorek JS & Kahne D. Inhibition of the β-barrel assembly machine by a peptide that binds BamD. Proc. Natl. Acad. Sci 112, 2011–2016 (2015). [PubMed: 25646443]
46. Ryu Y. & Schultz PG Efficient incorporation of unnatural amino acids into proteins in Escherichia coli. Nat. Methods (2006). doi:10.1038/nmeth864
47. Gibson DG et al. Enzymatic assembly of DNA molecules up to several hundred kilobases. Nat. Methods 6, 343–345 (2009). [PubMed: 19363495]
48. Roman-Hernandez G, Peterson JH & Bernstein HD Reconstitution of bacterial autotransporter assembly using purified components. Elife (2014). doi:10.7554/eLife.04234
49. Mastronarde DN Automated electron microscope tomography using robust prediction of specimen movements. J. Struct. Biol (2005). doi:10.1016/j.jsb.2005.07.007
50. Zheng SQ et al. MotionCor2: Anisotropic correction of beam-induced motion for improved cryo-electron microscopy. Nature Methods (2017). doi:10.1038/nmeth.4193
51. Rohou A. & Grigorieff N. CTFFIND4: Fast and accurate defocus estimation from electron micrographs. J. Struct. Biol (2015). doi:10.1016/j.jsb.2015.08.008
52. Wagner T. et al. SPHIRE-crYOLO is a fast and accurate fully automated particle picker for cryo-EM. Commun. Biol (2019). doi:10.1038/s42003-019-0437-z

53. Scheres SHW RELION: Implementation of a Bayesian approach to cryo-EM structure determination. J. Struct. Biol (2012). doi:10.1016/j.jsb.2012.09.006

54. Zivanov J, Nakane T. & Scheres SHW A Bayesian approach to beam-induced motion correction in cryo-EM single-particle analysis. IUCrJ (2019). doi:10.1107/S205225251801463X

55. Punjani A, Rubinstein JL, Fleet DJ & Brubaker MA CryoSPARC: Algorithms for rapid unsupervised cryo-EM structure determination. Nat. Methods (2017). doi:10.1038/nmeth.4169

56. Morin A. et al. Collaboration gets the most out of software. Elife (2013). doi:10.7554/eLife.01456

57. Pettersen EF et al. UCSF Chimera - A visualization system for exploratory research and analysis. J. Comput. Chem (2004). doi:10.1002/jcc.20084

58. Yang J. et al. The I-TASSER suite: Protein structure and function prediction. Nature Methods (2014). doi:10.1038/nmeth.3213

59. Zhang Y. I-TASSER server for protein 3D structure prediction. BMC Bioinformatics (2008). doi:10.1186/1471-2105-9-40

60. Roy A, Kucukural A. & Zhang Y. I-TASSER: A unified platform for automated protein structure and function prediction. Nat. Protoc (2010). doi:10.1038/nprot.2010.5

61. Emsley P. & Cowtan K. Coot: Model-building tools for molecular graphics. Acta Crystallogr. Sect. D Biol. Crystallogr (2004). doi:10.1107/S0907444904019158

62. Adams PD et al. PHENIX: A comprehensive Python-based system for macromolecular structure solution. Acta Crystallogr. Sect. D Biol. Crystallogr (2010). doi:10.1107/S0907444909052925

63. Chen VB et al. MolProbity: All-atom structure validation for macromolecular crystallography. Acta Crystallogr. Sect. D Biol. Crystallogr (2010). doi:10.1107/S0907444909042073

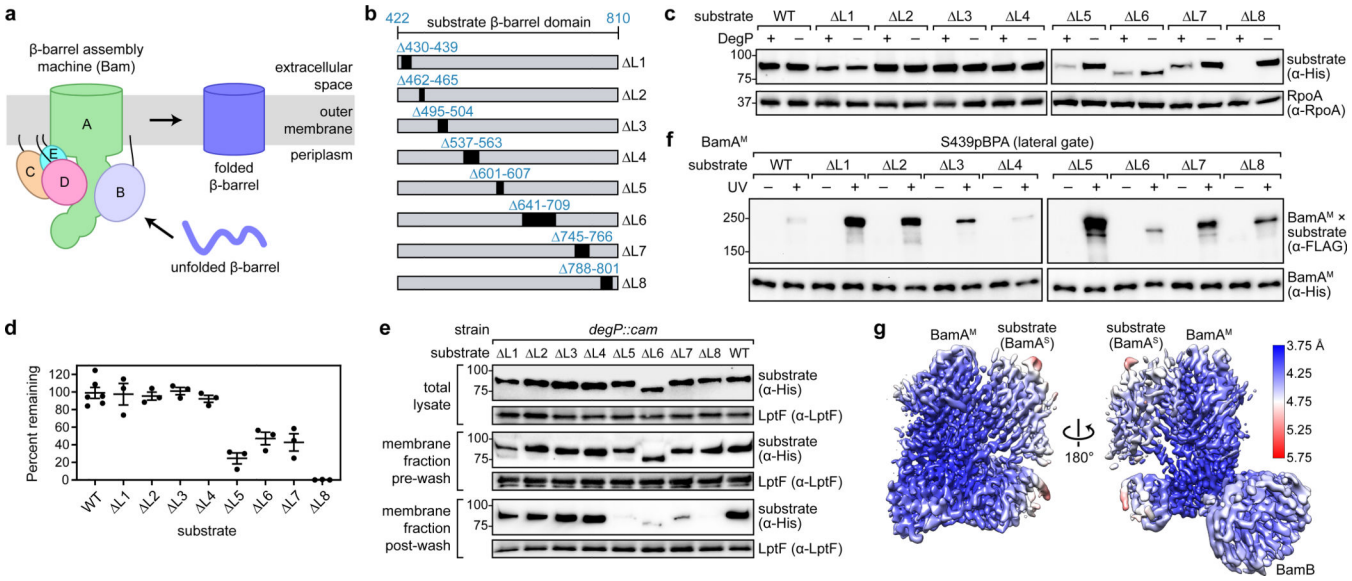

Figure 1 |. Deletion of extracellular loops causes substrates to stall at different stages of folding on the Bam complex.

a, Overview of β-barrel assembly by the Bam complex in Gram-negative bacteria. **b**, Schematic of engineered BamA substrates that contain extracellular loop deletions (BamA^{S}-ΔL). The residues deleted in each substrate are indicated. For simplicity, only the β-barrel domain of the substrate is shown. **c**, Expression levels of 6×His-tagged substrates in strains with or without *degP*. α-RpoA immunoblots are provided as loading controls. **d**, Quantification of immunoblotting data shown in **c**, with expression levels for each substrate calculated as the percent that remains when *degP* is expressed. The plotted data represent mean ± SEM from quantification data in **c** and additional independent replicates (n=6 for WT, n=3 for other substrates). **e**, Urea extraction of 6×His-tagged BamA^{S}-ΔL substrates. Samples from total cell lysates (top), membrane fractions before urea incubation (middle), and membrane fractions that remained after urea incubation (bottom) were analyzed. α-LptF immunoblots are provided as loading controls. Data shown are representative of results from two biological replicates. **f**, *In vivo* photocrosslinking of 6×His-tagged full-length BamA^{M}(S439pBPA) to 3×FLAG-tagged substrates. The strain lacking *degP* is used to ensure equal expression levels for all mutants, as shown in **c**. POTRA domains 3, 4, and 5 (Δ172–421) are removed in the substrates to prevent them from forming Bam complexes if they complete folding. Data shown are representative of results from three biological replicates. **g**, Cryo-EM map of substrate-bound Bam complex colored by local resolution.

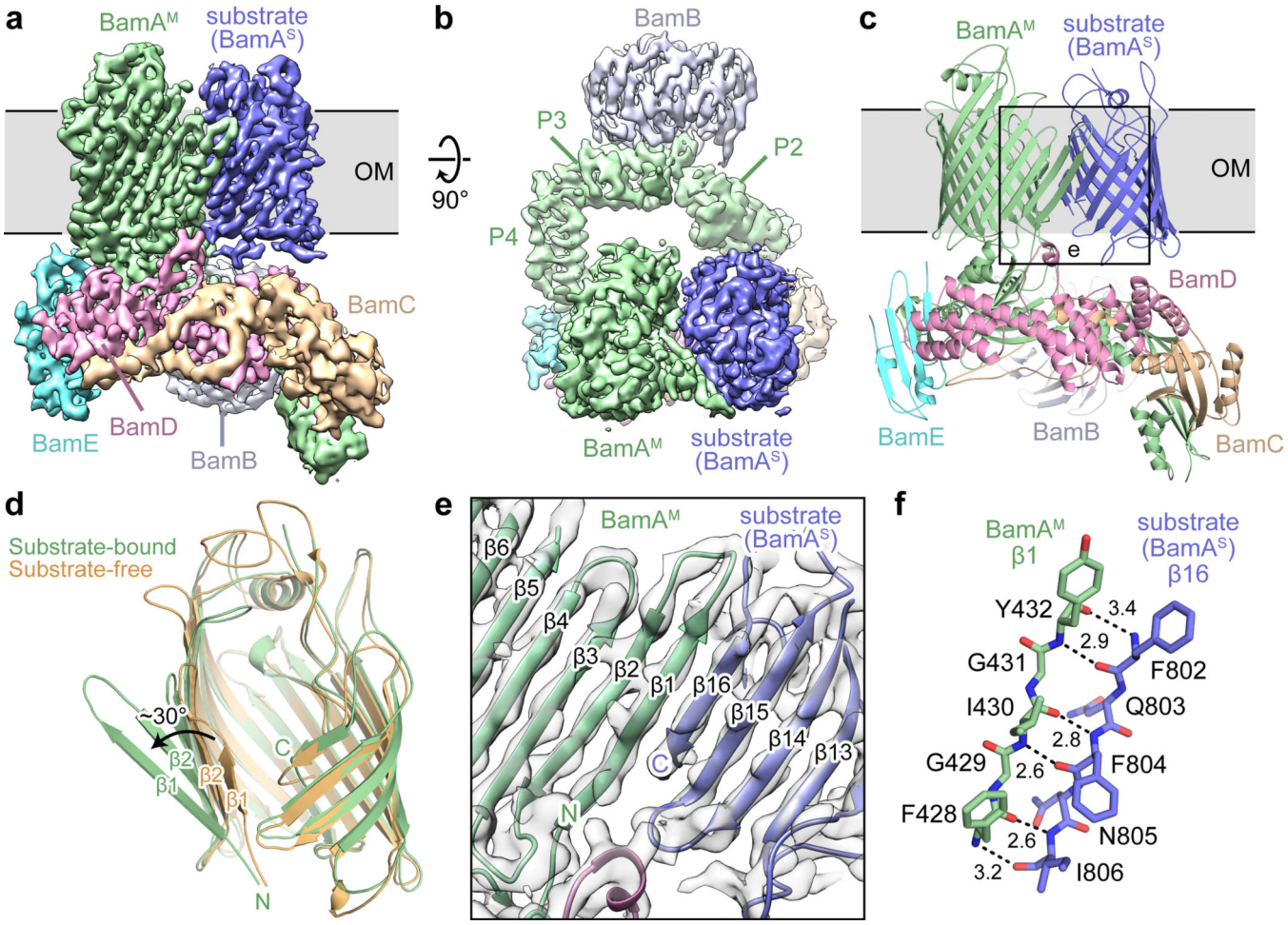

Figure 2 |. The N-terminal β-strand of BamA^{M} interacts with the C-terminal β-strand of the substrate by β-sheet augmentation.

a, Side view of the cryo-EM reconstruction of the Bam complex bound to the substrate (BamA^{S}-ΔL1). BamA^{M} is colored in green, BamB in silver, BamC in wheat, BamD in pink, BamE in cyan, and the substrate in blue. This color scheme is maintained in figures showing the cryo-EM structure. Approximate boundaries of the outer membrane (OM) are shown. BamC and POTRA domains 1 and 2 of BamA^{M} are shown at a lower contour level than the rest of the structure. **b**, Top-down view turned 90 degrees from view in **a**. P2, P3, and P4 refer to the POTRA domains of BamA^{M} that are visible in this view. **c**, Side view of the atomic model presented in the same orientation as in **a**. **d**, Overlay of BamA^{M} from substrate-bound complex (green) and from a substrate-free, lateral-open complex (orange, PDB ID: 5EKQ). **e**, Enlarged view of boxed region from **c**. The cryo-EM map is shown in gray. **f**, Interactions between β1 of BamA^{M} and β16 of the substrate shown in stick representation. Hydrogen bonds between the β-strands are shown as dashed black lines, and the bond lengths (Å) are labelled.

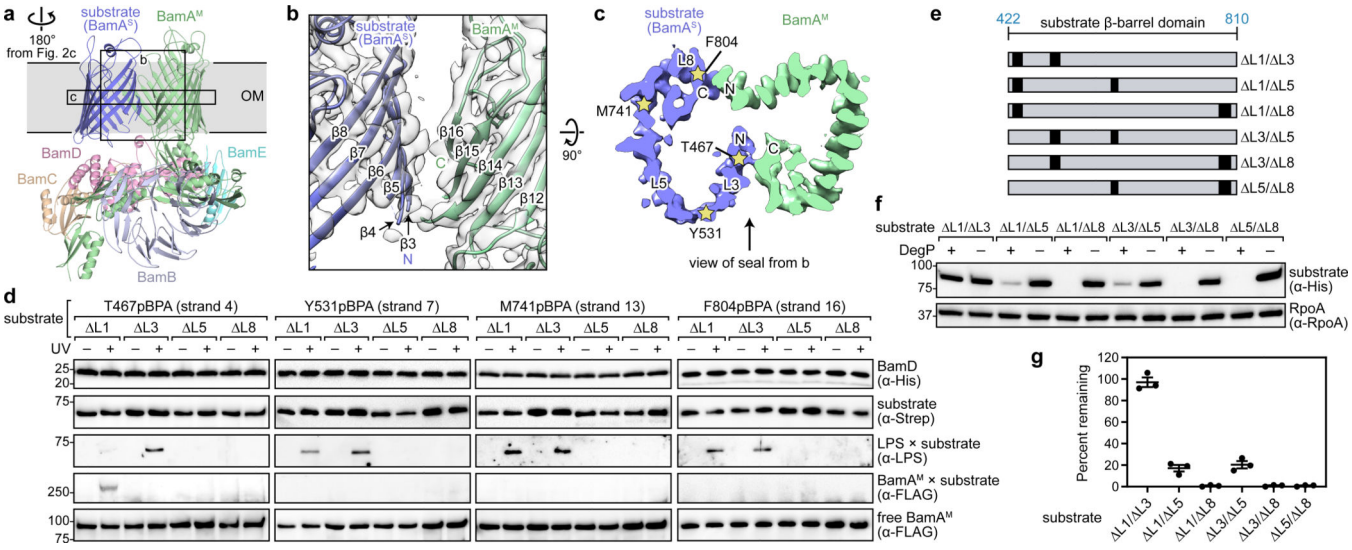

Figure 3 |. The hybrid barrel is asymmetric with the C-terminal β-strand of BamA^{M} and the N-terminal β-strand of the substrate unpaired in the membrane.

a, Side view turned 180 degrees from view in Fig. 2c to show interactions between the C-terminus of BamA^{M} and the N-terminus of the substrate. **b**, Enlarged view of boxed region from **a**. The cryo-EM map is shown in gray. This view shows the "seal" formed by the interaction of these ends of BamA^{M} and the substrate. **c**, Top-down view of a slice through the cryo-EM map, as indicated in **a**. The N- and C-termini of BamA^{M} and the substrate and approximate positions of L3, L5, and L8 within the substrate are indicated. Approximate positions of pBPA substitutions are indicated with stars. **d**, *In vivo* photocrosslinking of Strep-tagged BamA^{S}-ΔL substrates containing pBPA at positions T467, Y531, M741, or F804 and deletion of POTRA domains 3–5. Immunoblotting was performed using α-His, α-Strep, α-LPS, and α-FLAG antibodies to detect BamD (loading control), the substrates, substrate-bound LPS, and BamA^{M}, respectively. For α-FLAG immunoblot, a longer exposure (top, to detect crosslinks) and a shorter exposure (bottom) are shown. Data shown are representative of results from two biological replicates. **e**, Schematic of substrates in which two extracellular loops are removed. The residues removed are as given in Fig. 1b. **f**, Expression levels of substrates containing two loop deletions in strains with or without *degP*. α-RpoA immunoblot is provided as a loading control. **g**, Quantification of immunoblotting data shown in **f**, performed as in Fig. 1d. The plotted data represent mean ± SEM from quantification of data in **f** and additional independent replicates (n=3 for each substrate).

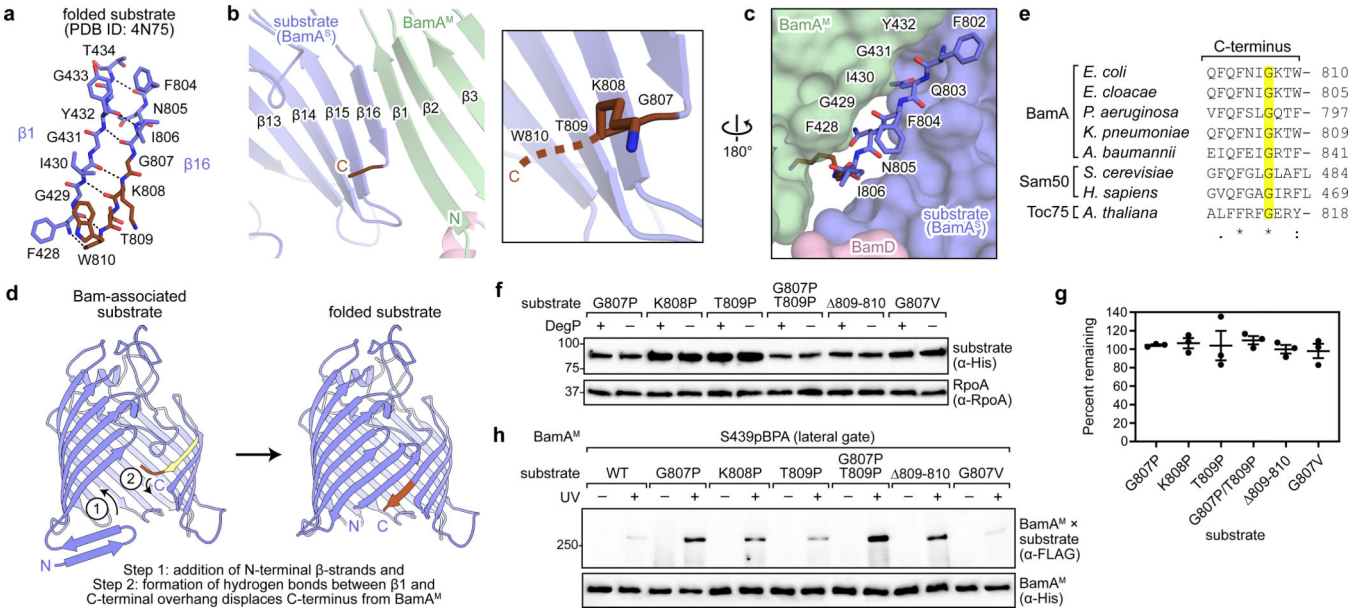

Figure 4 |. Release from BamA^M requires structural features of the substrate N- and C-termini that allow stepwise hydrogen bond exchange.

a, Interactions between β1 and β16 in the folded form of BamA (PDB ID: 4N75). Residues G807 to W810, which form an overhang in Bam-bound BamA^S (see below) are colored in brown. **b**, Interaction between BamA^M and the substrate (left). The view is from the interior of the two β-barrels. Residues within the substrate C-terminal overhang are in brown. The final two residues of the substrate could not be resolved, and their expected location is indicated with a dashed brown line (right). **c**, View of BamA^M-substrate interactions turned 180 degrees from view in **b** and similar to the view in Fig. 2e. With the exception of the C-terminal β-strand (β16) and overhang of the substrate, proteins are shown in semi-transparent surface representation. Residues in BamA^M β1 and substrate β16 are labelled. **d**, Model of substrate release involving pairing between the C-terminal overhang and N-terminal β-strand of the substrate. The substrate C-terminal overhang is in brown, and residues that interact with BamA^M in the Bam-associated substrate are in yellow. **e**, Alignment of the C-terminal regions of BamA and other Omp85 superfamily members. The invariant glycine is highlighted in yellow. **f**, Expression levels of 6×His-tagged substrates in strains with or without *degP*. α-RpoA immunoblots are provided as loading controls. **g**, Quantification of immunoblotting data shown in **f**, performed as in Fig. 1d. The plotted data represent mean ± SEM from quantification of data in **f** and additional independent replicates (n=3 for each substrate). **h**, *In vivo* photocrosslinking of 6×His-tagged full-length BamA^M(S439pBPA) to 3×FLAG-tagged substrates with POTRA domains 3–5 removed. Data shown are representative of results from three biological replicates.